REPORT DOCUMENTATION PAGE	*Form Approved* *OMB No. 0704-0188*

1. REPORT DATE *(DD-MM-YYYY)* 05/22/2018	**2. REPORT TYPE** Final	**3. DATES COVERED** *(From - To)* 30/09/2016-29/09/2017

4. TITLE AND SUBTITLE Development of high temperature PA/PBI polymer electrolyte membrane fuel cells	**5a. CONTRACT NUMBER** N62909-16-1-2241
	5b. GRANT NUMBER N62909-16-1-2241
	5c. PROGRAM ELEMENT NUMBER
6. AUTHOR(S) San Ping Jiang	**5d. PROJECT NUMBER**
	5e. TASK NUMBER
	5f. WORK UNIT NUMBER
7. PERFORMING ORGANIZATION NAME(S) AND ADDRESS(ES) Curtin University Kent St, Bentley 6102, WA Australia	**8. PERFORMING ORGANIZATION REPORT NUMBER**
9. SPONSORING/MONITORING AGENCY NAME(S) AND ADDRESS(ES) office of Naval Research Global 86 Blenheim Crescent Ruislip MX HA4 7HB United Kingdom	**10. SPONSOR/MONITOR'S ACRONYM(S)** ONR
	11. SPONSOR/MONITOR'S REPORT NUMBER(S)

12. DISTRIBUTION/AVAILABILITY STATEMENT

Distribution statement A

13. SUPPLEMENTARY NOTES

14. ABSTRACT

In this project, a new phosphotungstic acid impregnated mesoporous silica (PWA-meso-silica) and phosphoric acid doped polybenzimidazole (PA/PBI) composite membrane was developed for use in high temperature polymer electrolyte membrane fuel cells (PEMFCs) and achieved exceptional durability and high CO tolerance at elevated temperatures of 200 degrees. The fundamental reason is the in situ formed phosphosilicates can immobilize PA, forming PA/phosphosilicate nanoclusters that possess high proton conductivity and stability and substantially inhibits acid leaching. The success of such high temperature PEMFC is expected to accelerate the viability and practical application of liquid-fueled fuel cells.

15. SUBJECT TERMS

high temperature polymer electrolyte membrane fuel cells; mesoporous silica; tin oxides; PA/metal phosphate nanocluster; durability; direct methanol fuel cells; CO tolerance.

16. SECURITY CLASSIFICATION OF:			**17. LIMITATION OF ABSTRACT**	**18. NUMBER OF PAGES**	**19a. NAME OF RESPONSIBLE PERSON**
a. REPORT	**b. ABSTRACT**	**c. THIS PAGE**			
			SAR	42	**19b. TELEPHONE NUMBER** *(Include area code)*

Standard Form 298 (Rev. 8/98)
Prescribed by ANSI Std. Z39.18

Final report for US Office of Naval Research Global (ONRG)

Award Number: N62909-16-1-2241

Development of high temperature PA/PBI polymer electrolyte membrane fuel cells

Prof. San Ping Jiang

Date: 29 January 2018

Fuels and Energy Technology Institute and Department of Chemical Engineering, Curtin
University, Perth, WA 6102, Australia

TABLE OF CONTENTS

EXECUTIVE SUMMARY

Operation of polymer electrolyte membrane fuel cells (PEMFCs) at elevated high temperature has significant advantages over the low temperature PEMFCs and allows for a much better fuel impurity tolerance and substantially higher reaction kinetics as well as simplified water management and cooling systems. This is particularly important for the liquid fuels based PEMFCs. Membranes of phosphoric acid (PA) doped polybenzimidazole (PA/PBI) are among the most mutual and promising electrolyte systems in this connection, showing high proton conductivity at low water activity as well as good thermal and oxidative stability. However, PA/PBI membrane based cells are limited at temperatures up to about 160 °C. In the higher operating temperatures (>180-200 °C) the PA loss rate increases considerably and becomes unstable, eventually leading to acid depletion and failure of the cell system. It is a grand challenge to develop polymeric materials based membranes for operation at temperatures higher than 200°C.

In this project, we developed a phosphotungstic acid impregnated mesoporous silica (PWA-*meso*-silica) and phosphoric acid doped polybenzimidazole (PA/PBI) composite membrane for use in high temperature fuel cells and achieved exceptional durability under a constant current load of 200 mA cm^{-2} at 200 °C for over 2700 h. The fundamental role of PWA-*meso*-silica in enhancing the stability of the PA/PBI membrane has been investigated. The microstructure, the PA uptake, swelling ratio, mechanical property and conductivity of PA/PBI/PWA-*meso*-silica composite membranes depend on the loading of PWA-*meso*-silica. The results indicate that the optimum limit of PWA-*meso*-silica loading in the PA/PBI membranes is 15 wt%. Detailed analysis indicates that the mesoporous structure of the PWA-*meso*-silica framework disintegrates, forming phosphosilicate phases within the PBI polymeric matrix during fuel cell operation at 200 °C. The *in situ* formed phosphosilicates can immobilize a significant amount of PA, forming PA/phosphosilicate nanoclusters that possess high proton conductivity (e.g., 7.2×10^{-2} S cm^{-1} at 250 °C) and stability and substantially inhibits acid leaching. The substantially reduced acid leaching also alleviates the excess acid in the catalyst layer, reducing the detrimental effect of excess acid on the agglomeration of Pt catalysts especially in the cathode catalyst layer. These phenomena are responsible for the exceptional stability in proton conductivity of the PA/PBI/PWA-*meso*-silica composite membranes, as well as the significantly reduced agglomeration of Pt nanoparticles in the anode and cathode catalyst layers of PA/PBI/PWA-*meso*-silica composite membrane fuel cells.

The formation of phosphosilicate phase was studied in PA/silica mixture and the results indicate that phosphosilicate phase will form at 250 °C in air and is characterized by phosphosilicate nanoparticles covered by thin plate-like structure. The formation of highly porous, thin plate-like structure may be responsible for the immobilization of PA in the PBI polymer matric, leading to high proton conductivity and stability. The CO tolerance of PA/PBI/SiO_2 composite membrane cells is studied in the CO content of 0.66 to 16.7% in H_2. The results indicate that the CO tolerance increases with the operation temperature and the best results are obtained for the cells operated at 250°C with stable open circuit voltage and substantially reduced CO adsorption and poisoning on the cell performance. Direct methanol fuel cells based on PA/PBI/SiO_2 have been demonstrated, achieving 204 mW cm^{-2} at 260 °C in methanol fuel and reasonable stability. The results also show that silica powders can be used to replace *meso*-silica to fabricate PA/PBI/SiO_2 composite membrane cells with similar activity and stability.

SnO_2 has been added to the PA/PBI composite membrane and the results clearly show the formation of tin pyrophosphate phase between the doped PA and SnO_2 in the PA/PBI/SnO_2 composite membranes. Tin pyrophosphate phase shows a high proton conductivity of 5.5×10^{-2} S cm^{-1} at 300 °C with activation energy of 23.0 kJ mol^{-1} and good stability for 120 h at 250 °C. Preliminary results indicate that PA/PBI/SnO_2 composite membrane cells shows comparable performance and stability in direct methanol fuel, as compared to that of PA/PBI/SiO_2 composite membrane cells.

In conclusion, the current study demonstrates the feasibility of new metal phosphate proton conductor modified PA/PBI based composite membranes for operation at 250°C or higher with substantial increased CO tolerance and power output in CO containing H_2 and in liquid methanol fuel. The success of such high temperature PEMFC is expected to accelerate the viability and practical application of liquid-fueled PEM fuel cells as non-interrupted power sources in portable and communication electronic devices.

Keywords: high temperature polymer electrolyte membrane fuel cells; mesoporous silica; tin oxides; PA/metal phosphate nanocluster; durability; direct methanol fuel cells; CO tolerance.

1 INTRODUCTION

Fuel cells are electrochemical energy devices which convert the chemical energy of fuels into electricity, water and heat. According to the operation temperatures, fuel cells can be divided into two main groups; low temperature proton exchange membrane fuel cells (PEMFCs) and high temperature solid oxide fuel cells (SOFCs). PEMFC has the advantages of low operation temperature and fast start-up and shut down cycle, and has a great potential to be alternative power source for mobile and transportation applications. **Figure 1** shows the operation principle of a PEMFC[1].

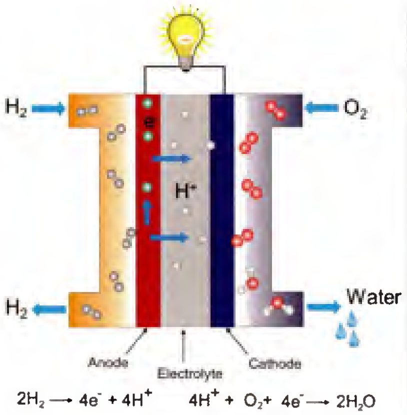

Figure 1. Operation principle of a proton exchange membrane fuel cell[1].

In PEMFCs, proton exchange membrane (PEM) is one of the most critical components for effective proton transportation and gas separation to prevent the mixing between fuel and oxidant. Perfluorosulfonic acid membranes such as Nafion® are the state-of-the-art PEMs with high chemical stability and outstanding proton conductivity at hydration condition. However, the proton conductivity of Nafion is extremely dependent on the hydration of the membrane, which requires a high level of relative humidity (RH) for the stable operation of Nafion membrane based fuel cells. Thus, Nafion based PEMFC can only be operated around room temperatures. Due to the low operation temperatures, pure H_2 (99.99%) is generally used as fuel as the Pt based electrocatalysts have a very low resistance to the fuel impurity such as CO. Although hydrogen provides the best performance and is the most efficient fuel in PEMFCs, the production, supply, transportation and storage issues associated with gaseous hydrogen fuels substantially retards the wide application and utilization of PEMFC technologies.

Alcohols based liquid fuels are easy to handle and shows higher volumetric energy density than hydrogen. For example, the volumetric energy density of methanol and ethanol is 15.6 and 20.9 MJ/L, respectively, which is substantially higher than 0.0108 MJ/L of H_2 gas under atmospheric pressure and 5.6 MJ/L of H_2 gas under 700 bar. As compared to pure hydrogen, alcohols such as methanol are byproducts of petrochemical industry and can also be obtained as biofuels. Thus, fuel cells based on the direct consumption of low cost and more readily available liquid fuels will be much more competitive than fuel cells based on gaseous hydrogen. However, despite the promising high energy density of liquid fuels, the power output of liquid fuels based cells is generally low due to the very low activity of Pt based electrocatalysts for the oxidation of alcohols such as methanol and ethanol at room temperatures.

Thus, the best solution to increase the power output of liquid fuels based PEMFCs is to increase the operation temperature. Operation of PEMFCs at elevated high temperatures would significantly enhance the reaction kinetics and allows for a much better fuel impurity tolerance [2]. The increased reaction kinetics will increase the power output and the high operation temperature will also significantly simplify the cooling and heat management systems and thus the stack design. The substantially enhanced impurity tolerance at high temperatures also allows the use of on board reformed hydrogen. The term *high temperature* used here refers to a temperature range from 100 to 350 °C, relative to the well-developed PEMFC technology typically operating at 80 °C or below. There have been substantial research activities in the development of high temperature PEMs. Among them, phosphoric acid (PA, H_3PO_4) doped polybenzimidazole (PBI)[3-5] or pyridine containing aromatic polyethers[6] are the most promising electrolyte systems in this connection, showing high proton conductivity at low water activity as well as good thermal and oxidative stability. Great progress has been achieved in this field and lifetimes of up to 18,000 h have been reported by several groups at constant current load as well as under dynamic operation at temperatures up to about 160 °C[7-12]. Nevertheless, at the operating temperatures higher than 160 °C, the loss rate of phosphoric acid increases considerably due to the thermal instability of PA, eventually leading to PA depletion and rapid proton conductivity decay. For instance, the PA leaching rate at the cathode at 190 °C has been found to be about an order of magnitude higher than at 160 °C[7]. As a result, the durability data reported in the literature at 190 – 200 °C do not extend to much more than a few hundred hours of operation.

We developed a novel composite membrane based on phosphotungstic acid ($H_3PW_{12}O_{40}\cdot nH_2O$, PWA) functionalized mesoporous silica (PWA-*meso*-SiO_2) and PA/PBI and demonstrated that the PA/PBI/PWA-*meso*-SiO_2 membranes show high proton conductivity and exceptional stability at 200°C for over 2700 h[13], a significant technological breakthrough in the development of HT-PEMFCs. The preliminary results are very encouraging but require further work to characterize the composite membrane, fundamentally understand the proton conductivity and thermal stability of the *in situ* formed phosphosilicate phases and to optimize the composition, structure and performance of PA/PBI/PWA-*meso*-silica membrane based fuel cells. Thus the objectives of the project are (1) to fully characterize mechanical, thermal and electrochemical properties and microstructure of the PA/PBI/PWA-*meso*-silica composite membrane; (2) fundamentally understand the mechanism and kinetics of the *in situ* formed phosphosilicates, proton conductivity, PA loading and property and structure of silica (e.g., mesoporous silica, nano-sized silica sphere with and without PWA functionalization); (3) test and evaluate the limits of CO tolerance and performance and power output of PWA-*meso*-SiO_2/PA/PBI membrane cells based on methanol fuel, and demonstrate the preliminary stability of the direct methanol fuel cells; and (4) investigate other metal/oxide based phosphate proton conducting carrier for composite PA/PBI membrane cells in order to further increase the proton conductivity, durability and operation temperature.

The report will be divided into two main part: the fundamental study of proton conductivity of *in situ* formed phosphosilicate and detailed characterization of PWA-*meso*-silica-PA/PBI membrane cells, and the development and preliminary studies of other metal phosphate proton conducting carrier based PA/PBI composite membranes for HT-PEMFCs.

2 EXPERIMENTAL

2.1 MATERIALS

Due to a high glass transition temperature (425 – 435 °C) and a high decomposition temperature (580 °C), PBI membrane was selected as the polymer matrix in this study. Dequalinium chloride hydrate (DCH), tetraethylorthosilicate (TEOS), triblock copolymer Pluronic surfactant P123 (EO_{20}-PO_{70}-EO_{20}), phosphotungstic acid, tine oxides and silica powder (15 and 30 nm) were purchased from Sigma-Aldrich, Australia. Ethanol (EtOH), hydrochloric acid (HCl, 32%), phosphoric acid (85 %), methanol and ethanol were obtained from Rowe Scientific Company, Australia. Pt/C (60 wt%) was purchased from Johnson Matthey, UK. Poly[2,2'-(*m*-phenylene)-5,5'-bisbenzimiazole] (*m*PBI, 6.1 wt% in dimethylacetamide) was sourced from Danish Power Systems, Denmark (inherent viscosity 0.95 dL g^{-1} at 30 °C and 500 mg dL^{-1} in 96 wt% H_2SO_4).

2.2 FABRICATION OF COMPOSITE MEMBRANE AND MEMBRANE-ELECTRODE-ASSEMBLY (MEA)

Meso-silica was fabricated using a conventional method. Pluronic P123 surfactant and HCl at specified ratios were dissolved in deionized water/ethanol solution, followed by the addition of TEOS. The mixture was stirred vigorously at 40 °C for 24 h and subsequently kept in an autoclave at 100 °C for 24 h. The collected powder was calcined at 650 °C for 6 h in air. The PWA-*meso*-silica with a loading of 40% PWA was obtained by impregnating PWA in *meso*-silica using a vacuum-assisted impregnation method[14]. The modification of PWA-*meso*-silica was conducted by dispersing the powder in a DCH solution (0.02 g mL^{-1} in methanol) followed by vigorous stirring for 4 h. The mixture was subsequently dried at 160 °C for 20 h yielding an off-white powder. The modified PWA-*meso*-silica powder was mixed with the *m*PBI solution. The suspension was mixed in ultrasonic bath for 20 h and cast onto a heated Petri dish starting at room temperature to 120 °C using a heating rate of 7 °C h^{-1}. The resultant composite membrane was treated with methanol at 50 °C in order to wash out the DCH modifier, followed by drying at 180 °C for 3 h. The loading of PWA-*meso*-silica in the PBI matrix was 5, 10, 15, 20, 30 and 40 wt%, while the thickness of the dry composite membrane was approximately 70 μm. Pristine PBI membrane (i.e., PWA-*meso*-silica loading was zero) with similar thickness was prepared by casting the PBI solution onto a heated petri dish starting at room temperature to 120 °C using a heating rate of 7 °C h^{-1} and was employed as a control group. The membranes were immersed in 85 wt% H_3PO_4 at room temperature for at least 2 weeks.

For the *in situ* formation of the immobilized proton conductors, the as-synthesized PBI composite membrane was immersed at a PA solution (85 wt.%) for one week. Then the membrane was heated at 200 °C for 24 h for the *in situ* formation of immobilized proton conductors within the polymeric matrix. The flow chart for the synthesis of *in situ* formed high temperature PEMs is shown in Fig. 2.

Phosphosilicate/PA particles were fabricated by mixing the *meso*-silica powder with phosphoric acid, followed by heating at 150 °C for 24 h and 250 °C for 24 h. One portion of the formed phosphosilicate/PA particles was washed by acetone to completely remove the phosphoric acid, and the resultant white powder was marked as pristine or pure phosphosilicate. Acetone treated phosphosilicate was mixed with phosphoric acid, forming mixed phosphosilicate and PA, denoted as phosphosilicate+PA. Phosphosilicate/PA particles formed without removal of PA by acetone washing were denoted as *in situ* formed phosphosilicate/PA or simply phosphosilicate/PA. The morphology and proton conductivity of phosphosilicate powder were also examined.

Gas diffusion electrodes were supplied by Danish Power Systems. The Pt/C catalyst was applied on a nonwoven carbon substrate (Freudenberg H2315 C2) using a spray technique and *m*PBI as binder. The loading of platinum and *m*PBI was 1.6 and 0.1 mg cm^{-2} for cathode and 0.1 and 0.1 mg cm^{-2} for anode, respectively. Membrane-electrode assemblies (MEA) with an active area of 4 cm^2 were fabricated by sandwiching the phosphoric acid doped membrane between two pieces of gas diffusion electrode followed by hot-pressing at 4.9 MPa and 180 °C for 10 minutes.

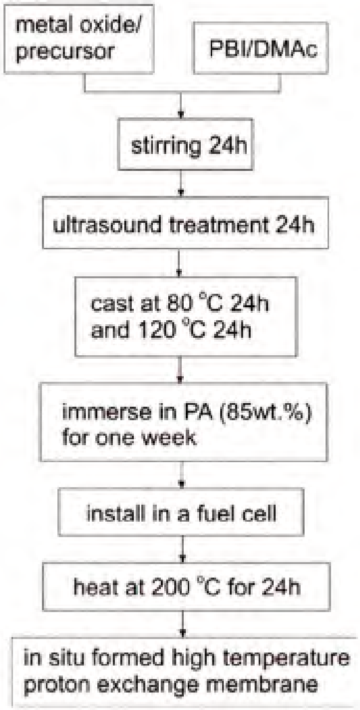

Figure 2. Flow chart for the *in situ* formed high temperature proton exchange membrane.

2.3 CHARACTERIZATION

Cross-section and surface of membranes were examined by scanning electron microscopy (SEM) using a Carl Zeiss EVO MA10 and transmission electron microscopy (TEM) using a Philips Tecnai F20 FEG-STEM at an accelerating voltage of 100 kV. The membrane cross-sections for SEM imaging were prepared by sandwiching the membrane samples between two pieces of non-woven carbon cloth followed by ion-milling using a Hitachi E-3500, and sputter coated with carbon. For transmission electron microscopy (TEM) the membrane samples were resin-mounted and sectioned using a Leica Ultracut UC6 ultramicrotome equipped with a diamond knife. Stress-strain curves were recorded using a Testometric Micro 350 under ambient conditions with a crosshead speed of 10.00 mm min^{-1}. The specimens were die-cut to a dog-bone shape with a gauge length and width of 28 and 2 mm, respectively. The Pt nanoparticles were examined using a JEOL 2100 TEM at an accelerating voltage of 120 kV. The Pt nanoparticles were dispersed in ethanol and subsequently placed on a copper grid. The

SEM imaging and electron dispersive X-ray spectroscopy (EDS) analysis of the Pt particles was carried out using JEOL 7100F. The microstructure of the samples was investigated by synchrotron small angle X-ray scattering (SAXS) with a camera length of 650 mm with a 3 GeV electron storage ring, Melbourne, Australia. The membranes were covered on the holes of a flat plate sample holder.

The MEAs were assembled in a single fuel cell hardware (active area 4.0 cm^{-2}) for the fuel cell performance measurements using an in-house built fuel cell test station. Hydrogen and air were supplied to the anode and cathode, respectively. Life time analysis of cells was undertaken in a continuous mode at 200 mA cm^{-2} and 200 °C using a flow rate of 45 SCCM for H_2 in anode and 176 SCCM for air in cathode. The impedance, as recorded on the fuel cells operated in parallel, was measured every 8 h. Electrochemical impedance spectroscopy (EIS) data were recorded periodically at open circuit voltage (OCV), 0.8 V, 0.7 V and 0.6 V in the frequency range 100 kHz to 0.1 Hz using a VersaStat 4 potentiostat from Princeton Applied Research. Phosphosilicate composite powders were pressed into pellets with the diameter of 25 mm for the proton conductivity test by EIS at a frequency range of 100 kHz to 1 Hz.

3. PART I – RESULTS OF PA/PBI/SiO_2 PEM FUEL CELLS

3.1 MESOPOROUS SILICA, SBA-15, BASED COMPOSITE MEMBRANE CELLS

3.1.1 MICROSTRUCTURE OF THE PBI/PWA-MESO-SILICA COMPOSITE MEMBRANE

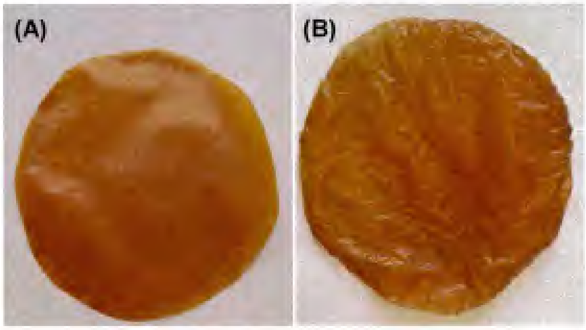

Figure 3. Optical photograph of the PBI/SiO_2 composite membrane (A) before and (B) after PA doping. The loading of the mesoporous SiO_2 (SBA-15) was 10 wt.%.

For the fabrication of the composite membrane, mesoporous silica (SBA-15 with space symmetry of P6mm) modified by dequalinium chloride hydrate were added into the PBI solution. Then the solution was casted in a petri dish by following the synthesis flow chart as sown in Fig.2 to obtain the PBI/SiO_2 composite membrane with 10 wt% SBA-15. The PBI/SiO_2 membrane is brown in colour and uniform,. as shown in Fig.3A, indicating that mesoporous silica particles are homogeneously distributed in the PBI polymer matrix. After the PA doping for one week, PA/PBI/SiO_2 composite membrane was obtained. The PA uptake of the membrane was 127 wt%, which is 24.4 % lower than that of the pristine PBI membrane. As shown in Fig.3B, the PA/PBI/SiO_2 composite membrane is intact and homogeneous. This indicates that adding SBA-15 additives does not cause visible change in the morphology of the PBI based membranes.

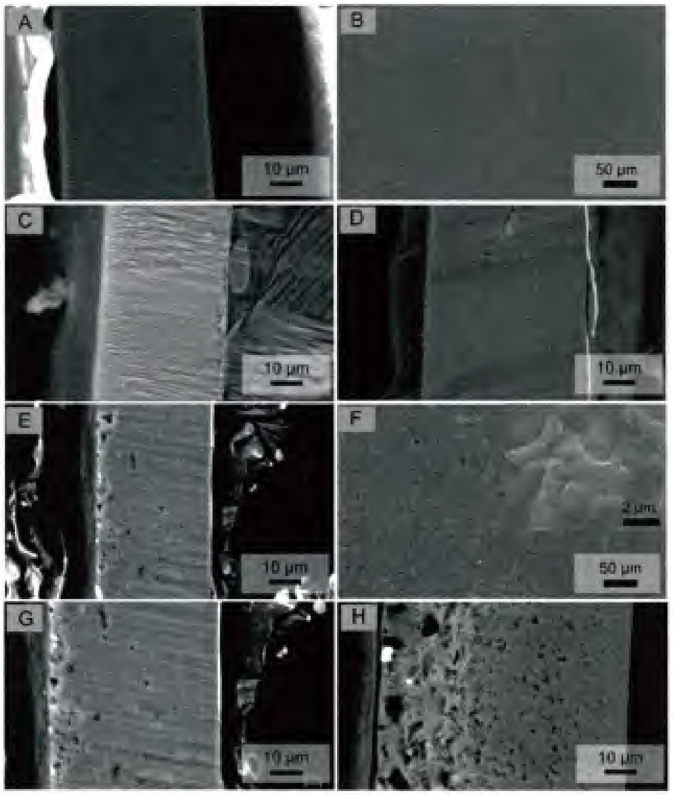

Figure 4. Scanning electron micrographs of cross-section and surface of PBI/PWA-*meso*-silica membranes with PWA-*meso*-silica loadings of (A,B) 0 wt%, (C) 5 wt%, (D) 10 wt%, (E,F) 15 wt%, (G) 20 wt% and (H) 40 wt%. Inset in (F) is an enlarged image of the light region of the surface of PBI/PBI-*meso*-silica with a loading of 15 wt% PWA-*meso*-silica.

Figure 4 shows the SEM images of the pristine PBI and PBI/PWA-*meso*-silica composite membranes. Pristine PBI membrane is characterized by a dense and smooth cross-section (Fig.4A) and surface (Fig.4B), indicating that the pristine PBI membrane is homogeneous. On the other hand, in the case of PBI/PWA-*meso*-silica composite membranes, the microstructure depends strongly on the loading of PWA-*meso*-silica filler. Homogeneous membranes were achieved when the loading of PWA-*meso*-silica in the PBI membrane was lower than 15wt% Fig.4C-F). The cross-section of the composite membrane with PWA-*meso*-silica loading lower than 15wt% is generally dense though some isolated pores were observed (Fig.4E). Isolated pores were also observed on the surface of the composite membrane (Fig. 4F). The formation of isolated pores is likely due to the presence of the inorganic filler and interface between the inorganic *meso*-silica particles and polymeric PBI matrix. The presence of two phases in the PBI/PWA-*meso*-silica composite membrane is also indicated by the backscattering electron image as shown in Fig. 4F. The phase in light colour corresponds to the PWA-*meso*-silica particles and the particle size is 1-2 µm (see the inset of Fig. 4F), while the dark phase is the PBI matrix. However, with loadings of PWA-*meso*-silica higher than 15 wt%, anisotropic structures and pore formation were observed (Fig.4G and H), likely due to the agglomeration of the inorganic component at high concentrations. The results indicate that the composite membrane with 15 wt% PWA-*meso*-silica loading would meet the microstructure and morphology properties as required in PEM fuel cells.

To observe the dispersion of PWA-*meso*-silica in the PBI matrix, a film was cut from a PBI composite membrane with 15 wt% PWA-*meso*-silica by a microtome. Figure 5 shows TEM images of the PBI/PWA-*meso*-silica composite. From the TEM backscattered electron image, two phases were clearly observed (Fig. 5A). Mesoporous structure in [001] and [100] directions was observed in the light region of the membrane (Fig.5B), which corresponds to the structure of mesoporous silica. EDS analysis of the mesoporous region identifies the elements of Si and W (Fig. 5C), confirming the presence of PWA-*meso*-silica in the composite membranes.

Figure 5. (A,B) TEM image of the PBI/PWA-*meso*-silica composite membrane and (C) the EDS spectrum of the rectangular area in (A). PWA-*meso*-silica loading in the composite membrane was 15 wt%.

3.1.2 PHOSPHORIC ACID UPTAKE AND MECHANICAL PROPERTIES OF THE COMPOSITE MEMBRANES

PBI membranes were equilibrated in 85% PA at room temperature for two weeks to ensure that PA doping level reached an equilibrium in the composite membranes. PA uptake of pristine PBI membrane was 341wt%, corresponding to about 10.5 PA per polymer repeat unit. In the case of PBI/PWA-*meso*-silica membranes, the PA doping level decreased with the increase in the loading of PWA-*meso*-silica fillers. In the case of PBI/PWA-*meso*-silica membrane with 15 wt% filler, the PA uptake was 242 wt%, corresponding to 7.5 PA per polymer repeat unit. The swelling volume of the composite membrane also decreased with the increase in the filler loadings, varied in the range of 167 % to 100 %. For PBI/PWA-*meso*-silica membrane with 15 wt% filler, the swelling ratio was 137 %, which is 43.3 % lower than that of the pristine PBI membrane. This indicates the positive influence of the PWA-*meso*-silica filler on the swelling volume of the composite membrane. Table 1 lists the PA doping level and swelling ratio of pristine PBI and PBI/PWA-*meso*-silica composite membranes.

Table 1. Physical properties of PBI and PBI/PWA-*meso*-silica composite membrane including elastic modulus, phosphoric acid uptake and volume swelling after phosphoric acid doping.

PBI/PWA-*meso*-silica Membrane wt% filler	Elongation, %		Elastic modulus, MPa		PA uptake, wt%	Volume swelling, vol%
	Before PA doping	After PA doping	Before PA doping	After PA doping		
0%	10.4±4.7	58.3±22.1	3384±409	52.3±0.6	341	242
5%	11.0±3.4	114.5±21.0	2755±367	54.3±8.8	308	167
10%	3.2±0.8	108.8±11.3	1873±323	41.8±4.4	284	163
15%	4.4±0.6	88.3±39.5	1992±282	33.0±12.3	242	137
20%	2.3±0.2	122.7±13.6	2350±398	53.3±4.4	226	128
30%	2.7±1.2	126.9±29.2	1878±654	32.9±11.8	219	130
40%	1.4±0.2	91.5±16.5	1589±409	25.0±7.5	215	100

Mechanical properties of a membrane are a critical aspect of a membrane's suitability for use in fuel cells. Mechanical properties of the PBI composite membranes before and after PA-doping were tested and the results are shown in Fig.6. Before PA doping, the pristine PBI membrane shows outstanding mechanical properties and dimensional stability (Fig. 6A and B). The elastic modulus of the pristine PBI membrane was 3384±409 MPa and its elongation was 10.4±4.7 %. However, with the addition of PWA-*meso*-silica in the PBI membrane, the mechanical strength of the composite membrane generally decreased. For example, for composite mebrane with 15 wt% PWA-*meso*-silica, the mechanical strength slightly decreases to 1992±282 MPa and the elongation reduces to 4.4±0.6 % (Fig.6A and B). This may be due to the presence of isolated pores in the composite membrane. After PA doping, the mechanical strength of the pristine PBI membrane is substantially diminished (Fig.6C and D) and the elastic modulus is decreased from 3384±409 MPa to 52.3±0.6 MPa (Table 1). However, the elongation of the PA/PBI membrane is increased from 10.4±4.7 % to 58.3±22.1 %. This is probably due to the swelling of the membrane and the reduced intermolecular forces among the polymer macromolecules. The elastic modulus of the PA/PBI/PWA-*meso*-silica composite was in the range of 25.0 – 54.3 MPa, comparable to 52.3 MPa of the pristine PA/PBI membrane (Fig.6D). The elongation of the composite membranes varied between 88.3 % to 126.9 %, also comparable to the pristine PA/PBI membrane (Fig.6C). The close mechanical and elastic properties between PA/PBI/PWA-*meso*-silica and pristine PA/PBI membranes indicate that addition of PWA-*meso*-silica does not significantly vary the mechanical and elastic properties of PA/PBI membranes, demonstrating the excellent fabrication and processing capability potential of the PA/PBI/PWA-*meso*-silica inorganic-organic composite membranes, a significant advantage as compared to inorganic PEMs[14, 15].

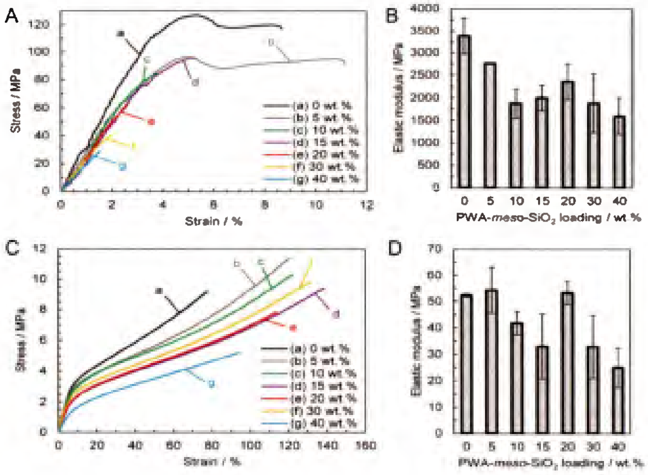

Figure 6. Stress-strain curves and corresponding elastic modulus for the PBI/PWA-*meso*-silica composite membranes with PWA-*meso*-SiO_2 loadings of 0-40 wt% before (A,B) and after (C,D) phosphoric acid doping. The heights of the gray bars in (B,D) represent the average values and the standard deviations are indicated by the error bars.

As shown early[13], in the PWA-*meso*-silica loading range of 0 - 20 wt%, the effect of filler on the conductivity of the PA/PBI/PWA-*meso*-silica composite membranes is relatively small and with further increase of the filler loading, the proton conductivity of the composite membrane decreases. This may be due to the deteriorated microstructure as shown in Fig.4. Taking into account the microstructure, the PA uptake, swelling ratio, mechanical and conductivity properties, the optimum limit of PWA-*meso*-silica loading in the PA/PBI membranes has been determined to be 15 wt%. Thus in following sections, only the electrochemical performance of the composite membrane cells with 15 wt% PWA-*meso*-silica fillers is characterized and discussed.

3.1.3 CELL PERFORMANCE AND PROTON CONDUCTIVITY OF PA/PBI/PWA-MESO-SILICA MEMBRANES

Figure 7 shows the performance and stability of PA/PBI and PA/PBI/PWA-*meso*-silica composite membrane fuel cells at 200 °C and a constant current load of 200 mA cm^{-2}. The loading of PWA-*meso*-silica fillers in the composite membrane was 15 wt%. The PA/PBI membrane fuel cell is not stable and degrades significanty upon polarization at 200 mA cm^{-2} (Fig. 7A). The initial cell voltage was 0.70 V and fell to 0.52 V after polarization at 200 mA cm^{-2} for 1450 h with a degradation rate of 129 μV h^{-1}. This was followed by a rapid decline in cell voltage, acquiring a cell potential of close to zero after polarization for 2400 h representing a degradation rate of 705 μV h^{-1}. These values are similar to results reported by Li et al.[16]

for the durability of a PA/PBI membrane fuel cell limited to 1000 h of operation under similar conditions to the present study. By contrast, the PA/PBI/PWA-*meso*-silica composite membrane fuel cell showed a very stable performance. The initial cell voltage was 0.68 V and reached 0.53 V after polarization at 0.2 A cm^{-2} and 200 °C for 2700 h. Except for an initial reduction in performance during the first 500 h, the cell voltage was relatively stable during the next 2200 h and the cell voltage degradation rate was 27 μV h^{-1}, which is significantly better than the degradation rate of 60 μV h^{-1} that has been reported previously on a commercial PA/PBI membrane fuel cell operated at a lower temperature of 190 °C[7].

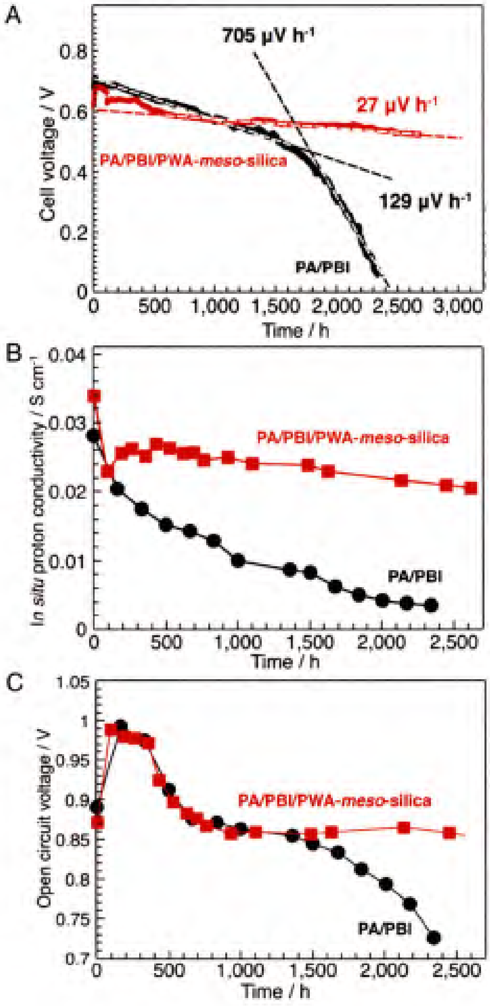

Figure 7. (A) Long-term stability testing of pristine PA/PBI membrane and PA/PBI/PWA-*meso*-silica composite membrane cells; (B) plots of the *in situ* membrane conductivity and (C) open circuit voltage. The fuel cells were tested at a constant current density of 200 mA cm^{-2} and 200 °C in H_2/air under anhydrous conditions. PWA-*meso*-silica loading in the composite membrane was 15 wt%.

The initial proton conductivity of the PA/PBI membrane during operation at 200 °C was 28 mS cm^{-1}, slightly lower than 34 mS cm^{-1} for the PA/PBI/PWA-*meso*-silica composite membrane under identical conditions (Fig.7B). This is generally in line with the reported conductivity of 68 mS cm^{-1} for PBI membranes with PA doping level of 5.6 at 200 °C and 5% RH[17]. During fuel cell operation, the proton conductivity of the PA/PBI membrane decreased rapidly to 3.5 mS cm^{-1} after polarization for 2340 h, a reduction of ~90% of the initial conductivity of the membrane. This rapid decrease in proton conductivity is clearly due to membrane degradation and/or acid leaching from the membrane[18, 19]. By contrast, except for the initial decrease, the proton conductivity of the PA/PBI/PWA-*meso*-silica composite is very stable and oscillates in the range of 21 to 23 mS cm^{-1} during a test period of 2700 h. These results demonstrate that the presence of PWA-*meso*-silica inorganic particles effectively inhibits the deterioration in proton conductivity of the PA/PBI membrane, probably through the suppression of acid leaching from the membrane. This inhibition effect is also confirmed by the stable open circuit voltage of the PA/PBI/PWA-*meso*-silica composite membrane fuel cell during 2600 h operation, as shown in Fig. 7C. On the other hand, the OCV of the PA/PBI fuel cell sharply dropped from 0.89 V to 0.73 V after operation for 2340 h.

The power output of the PA/PBI and PA/PBI/PWA-*meso*-silica membrane fuel cells was evaluated during the stability tests at 200 °C and the results are presented in Fig. 8. The initial peak power density of the PA/PBI membrane fuel cell was 407 mW cm^{-2}, which is comparable with reported results. For example, Jin et al studied the performance of PA/PBI with and without addition of $Sn_{0.95}Al_{0.5}P_2O_7$ and reported peak power density of 369 mW cm^{-2} in H_2/O_2 for PA/PBI membrane cells and 440 mW cm^{-2} in H_2/air for PA/PBI/$Sn_{0.95}Al_{0.5}P_2O_7$ composite membrane cell measured at 200 °C with overall Pt catalyst loading of 8 mg cm^{-2} [20]. The initial peak power density of the PA/PBI/PWA-*meso*-silica membrane fuel cell was 386 mW cm^{-2}, very close to that of the PA/PBI membrane fuel cell (Fig.8A). However, the power output of the PA/PBI membrane fuel cell diminished rapidly after polarization for 1750 h (Fig.8B), with the peak power density of 82.3 mW cm^{-2} representing a much lower value than the 224.8 mW cm^{-2} value obtained with a PA/PBI/PWA-*meso*-silica composite membrane fuel cell. After polarization for 2400 h (Fig.8C), the peak power density of PA/PBI membrane cell was 48.4 mW cm^{-2}, only 11.9 % of the initial power output of this fuel cell. By contrast, the peak power density of the PA/PBI/PWA-*meso*-silica composite membrane fuel cell was 198 mW cm^{-2} under the same test conditions, substantially higher than that of PA/PBI membrane cell. Table 2 lists the peak power density of PA/PBI and PA/PBI/PWA-*meso*-silica composite membrane fuel cells as a function of polarization time at 200 °C.

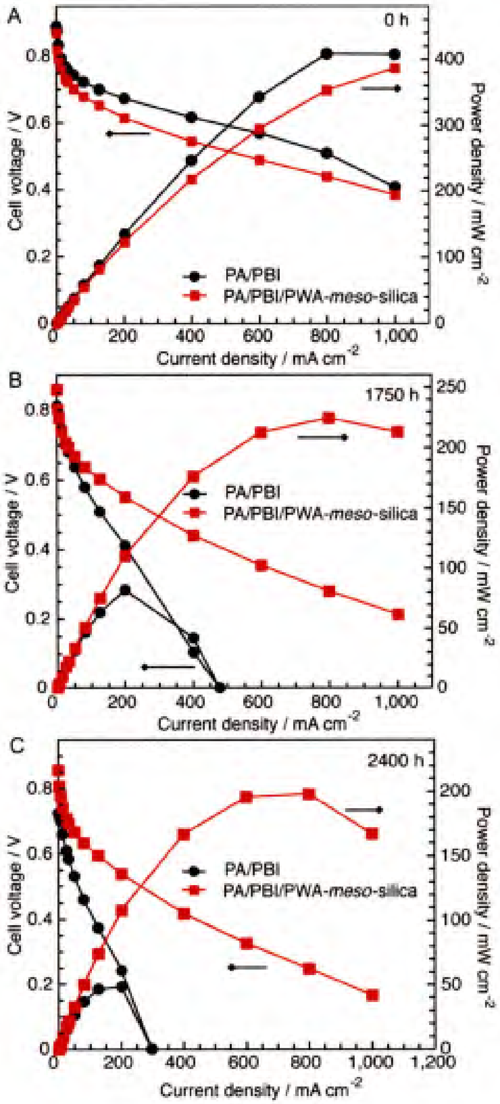

Figure 8. Polarization curves of PA/PBI and PA/PBI/PWA-*meso*-silica membrane fuel cells at 200 °C after polarization at a constant current density of 200 mA cm^{-2} for (A) 0 h; (B) 1750 h; and (C) 2400 h. PWA-*meso*-silica loading in the composite membrane was 15 wt%.

Polarization resistance and ohmic resistance of pristine and composite membrane fuel cells were determined by EIS during the stability testing at 200 °C (see Fig.9). It illustrates that the ohmic resistance of the PA/PBI membrane cell increases from 0.36 Ω cm^2 to 1.78 Ω cm^2, an increase of 391 % in just 320 h, while the increase in the ohmic resistance of the composite increases is much smaller (Fig. 9A). After 2700 h, the ohmic resistance of the composite membrane cell only increased from 0.16 Ω cm^2 to 0.33 Ω cm^2 which is much lower than 1.78 Ω cm^2 measured on PA/PBI membrane cell after only 320 h (Fig.9B). Most interesting, the polarization resistance of the PA/PBI membrane cell increased from 0.52 to 0.71 Ω cm^2 within 320 h, while it increased from 0.32 to 0.48 Ω cm^2 during 2700 h for the composite membrane cell. The increase in the polarization resistance for the PA/PBI/PWA-*meso*-silica composite membrane cells is also much smaller as compared to PA/PBI membrane cells. This suggests that the addition of the inorganic *meso*-silica filler also contributes to a stabilization of the Pt/C catalyst electrode. The results demonstrate that performance degradation in PA/PBI membrane fuel cells is primarily related to increases in the ohmic resistance of the cell and changes in the electrode polarization resistance to a less degree.

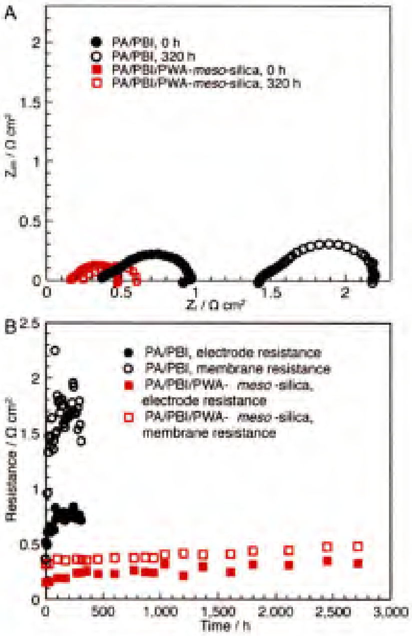

Figure 9. (A) EIS Nyquist plots and (B) membrane resistance and electrode polarization resistance of the PA/PBI membrane and PA/PBI/PWA-*meso*-silica membrane fuel cells as a function of polarization time at 200 mA cm^{-2} and 200 °C in H_2/air under anhydrous conditions. PWA-*meso*-silica loading in the composite membrane was 15 wt%.

Table 2. Peak power density, membrane and electrode resistance and Pt particle size of anode and cathode of PA/PBI and PA/PBI/PWA-*meso*-silica composite membrane fuel cells before and after stability test at 200 mA cm^{-2} and 200 °C.

Cell	Powder density / mW cm^{-2}			Resistance / Ω cm^2						Pt particle size / nm		
				Membrane			Electrode				Anode	Cathode
	0 h	1750h	2400 h	0 h	320 h	2700h	0 h	320h	2700h	0 h	2400-2700 h	
PA/PBI	407	82.3	48.4	0.36	1.78	-	0.52	0.71	-	3.4	5.7	10.5
PA/PBI/PWA-*meso*-silica	386	224.8	198	0.16	0.24	0.33	0.32	0.36	0.48	3.4	4.0	5.7

3.1.4 MICROSTRUCTURE OF THE COMPOSITE MEMBRANE AND PT ELECTROCATALYST AFTER STABILITY TEST

Figure 10 shows SEM images of the PA/PBI/PWA-*meso*-silica composite membrane after 2700 h of fuel cell testing. The surface of the composite membrane is generally smooth with, in some instances, isolated areas of aggregated particles in the size range of 20 - 50 nm (Fig.10A and B). However, SAXS analysis could not detect the mesoporous silica particulate phases in the PBI matrix. After operation of the fuel cell, the unique SAXS peaks of *meso*-silica corresponding to the planes of (100), (110) and (200) had vanished (Fig.10C), indicating the disintegration of the mesoporous structure of silica phase during the fuel cell operation at 200 °C. Pristine PBI shows a broad peak in the range of 15 – 30°, indicating the amorphous structure of the polymer membrane[21]. In the case of PA/PBI membrane cells, two new peaks around 20° and 27° were detected after operation at 200 °C for 2400 h (Fig.10D), corresponding to the P_2O_7 and P_2O_5, respectively. This is likely due to the decomposition of phosphoric acid in the PA/PBI membrane. Very different from PA/PBI membrane cells, in addition to XRD peaks of P_2O_7 and P_2O_5, two new peaks around 22.9° and 25.0° were detected for the PA/PBI/PWA-*meso*-silica membrane after the fuel cell test and have been identified with $Si_5O(PO_4)_6$ phase (JCPDF card 04-011-0823)[22]. This indicates the *in situ* formation of phosphosilicate phase during the PA/PBI/PWA-*meso*-silica membrane fuel cell operation at 200 °C. The results imply that the disintegration of the mesoporous silica phase is due to the reaction between mesoporous silica and PA and the formation of phosphosilicate during operation of the fuel cell.

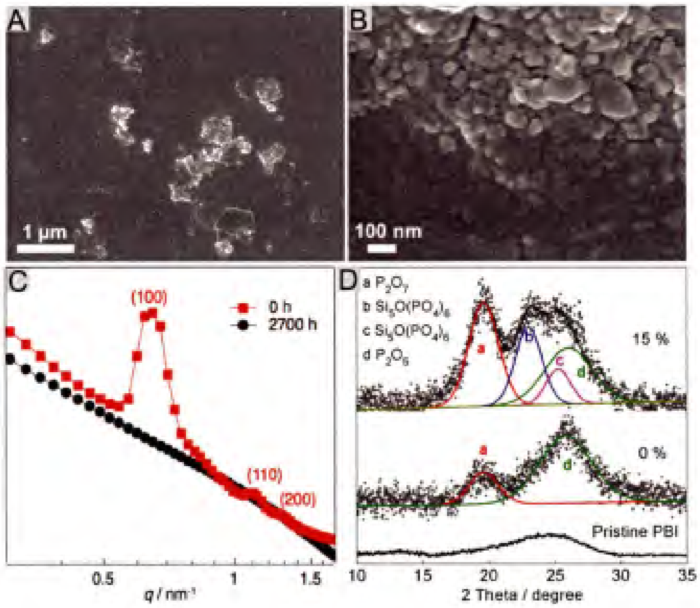

Figure 10. (A, B) SEM images of the surface of a PA/PBI/PWA-*meso*-silica composite membrane after 2700 h of fuel cell testing, (C) SAXS profiles of the PA/PBI/PWA-*meso*-silica composite membrane before and after stability testing, and (D) XRD profiles of pristine PBI, PA/PBI and PA/PBI/PWA-*meso*-silica composite membranes after fuel cell stability testing. PWA-*meso*-silica loading in the composite membrane was 15 wt%.

Matsuda *et al.*[23] studied the synthesis of phosphosilicate phase by phosphoric acid and tetraethoxysilane and revealed the detection of Si-O-P bonds and the formation of phosphosilicate phase, $Si_5O(PO_4)_6$. Thus, during the operation of PA/PBI/PWA-*meso*-silica membrane cell at 200 °C, phosphoric acid molecules would react with mesoporous silica, leading to the disintegration of the mesoporous framework and consequently the formation of phosphosilicate, similar to that reported by Matsuda et al. for the reaction between phosphoric acid and tetraethoxysilane [23].

$$5SiO_2 + 6H_3PO_4 \rightarrow Si_5O(PO_4)_6 + 9\ H_2O \qquad (1)$$

Moreover, the Si-O-P bonds are expected to enhance the retention of phosphoric acid molecules in the phosphosilicate and thus improve the proton conductivity of the composite membrane.

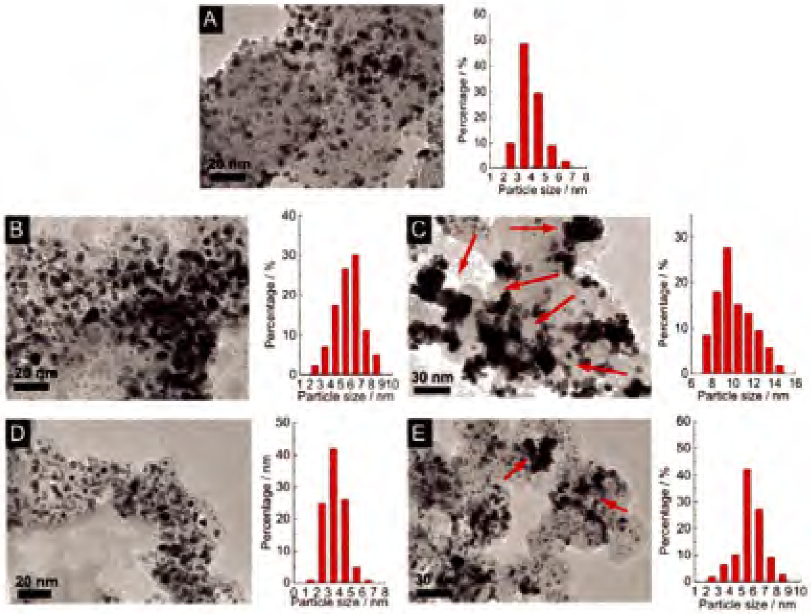

Figure 11. TEM images and related size distribution of (A) original Pt/C catalyst before testing, (B) Pt/C anode and (C) Pt/C cathode of PA/PBI membrane fuel cells, and (D) Pt/C anode and (E) Pt/C cathode of PA/PBI/PWA-*meso*-silica composite membrane fuel cells. The cells were tested at 200 °C with a current load of 200 mA cm^{-2} for 2400 h with the PA/PBI membrane fuel cell and 2700 h with the PA/PBI/PWA-*meso*-silica membrane fuel cell. PWA-*meso*-silica loading in the composite membrane was 15 wt%.

The microstructure and particle size of Pt electrocatalysts before and after the stability testing were examined by TEM with the results presented in Fig. 11. The average particle size of Pt catalyst of the fresh-prepared MEAs was 3.4 nm (Fig. 11A). However, the size of Pt nanoparticles increased significantly after the long-term stability testing at 200 °C. In the case of PA/PBI membrane cells, the average Pt particle size was 6.7 and 10.5 nm for anode and cathode after testing for 2400 h (Fig.11B and C), respectively, much larger than the original size of 3.4 nm of the Pt/C catalysts. This is consistent with the observed significant agglomeration of Pt-based catalysts of PA/PBI membrane cells operated at a high temperature of 190 °C[10]. Moreover, the increase in the agglomeration of Pt nanoparticles in the cathode is much higher than observed in the anode. This may be due to a higher water vapour pressure produced in the cathode layer as compared to the anode layer of the pristine PA/PBI membrane based fuel cells during operation [24]. In the case of the PA/PBI/PWA-*meso*-silica composite membrane fuel cell, the average particle size of the Pt catalyst was 4.0 and 5.7 nm in the anode and cathode layers after testing for 2700 h (Fig.11D and E), respectively, significantly smaller than those in the pristine PA/PBI membrane fuel cell. These results demonstrate that the addition of the PWA-*meso*-silica filler in PBI also increases the stability of the Pt catalyst in the electrodes, particularly in the cathode layer. However, EDS analysis indicates the presence of C, O, Pt and P but not W in the cathode of both PA/PBI and PA/PBI/PWA-*meso*-silica membrane fuel cells (see Fig.12) after long-term stability testing. This suggests that the PWA-*meso*-silica inorganic additive remains within the PBI matrix.

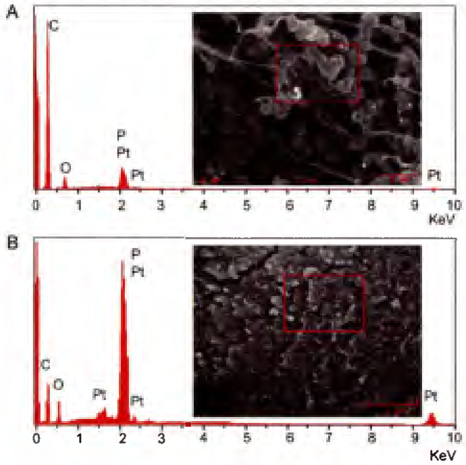

Figure 12. EDS of the catalyst layer in cathodes of (A) PA/PBI membrane fuel cell and (B) PA/PBI/PWA-*meso*-silica membrane fuel cell after the long-term stability test at 200 °C. Inset is the SEM image of the catalyst layer. PWA-*meso*-silica loading in the composite membrane was 15 wt%.

3.1.5 ROLE OF PWA-MESO-SILICA IN THE COMPOSITE MEMBRANE

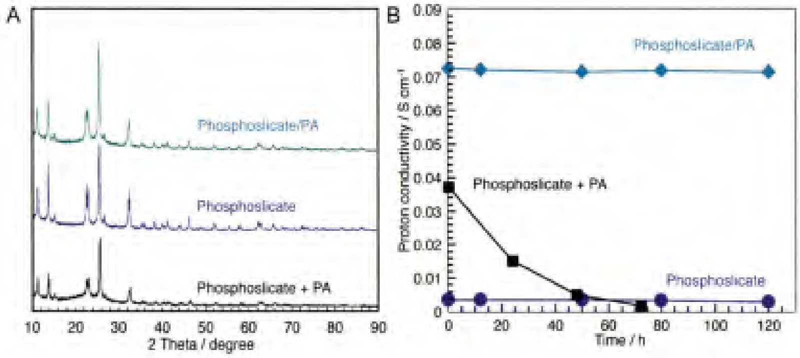

Figure 13. (A) XRD and (B) proton conductivity data for phosphosilicate, a mixture of phosphosilicate and phosphoric acid (phosphosilicate + PA) and *in situ* synthesized phosphosilicate/PA samples measured at 250 °C under anhydrous conditions.

The interaction between phosphoric acid and silicate was studied in order to fundamentally understand the role of PWA-*meso*-silicate in the PA/PBI/PAW-*meso*-silicate composite membranes. Fig.13 presents XRD phase, proton conductivity and stability data of pure phosphosilicate, *in situ* formed phosphosilicate in PA (phosphisilicate/PA) and a simple mixture of pure PA and phosphosilicate (phosphisilicate+PA), all measured at 250 °C under anhydrous conditions, noting that the phosphosilicate phase, $Si_5O(PO_4)_6$ can be prepared by condensation of Si-OH and P-OH on heating of a SiO_2-H_3PO_4 mixture at about 200 °C[25]. The purpose of this stability test at 250 °C was to accelerate the degradation process of these samples.

The results shows that the proton conductivity of the pure phosphosilciate phase is low, 3.6×10^{-3} S cm^{-1} at 250 °C, but is stable (Fig.13B), which is in agreement with data reported elsewhere[23]. When pure phosphosilicate was mixed with phosphoric acid, the proton conductivity of the mixture increases to 3.7×10^{-2} S cm^{-1} at 250 °C. However, the stability in proton conductivity of the mixture is very poor with a decrease to 1.7×10^{-3} S cm^{-1} after testing for 72 h, an order of magnitude lower than the initial conductivity. This is probably due to the condensation and separation of PA from the phosphosilicate phase at elevated high temperatures. The condensation of short-chain phosphate would be irreversible in a dry atmosphere condition, resulting in a diminution in proton conductivity[26]. On the other hand, the *in situ* formed phosphosilicates or phosphosilicate/PA showed a high proton conductivity of 7.2×10^{-2} S cm^{-1} at 250 °C, more than an order of magnitude higher than 3.6×10^{-3} S cm^{-1} with the pure phosphosilicate phase. Most importantly, the proton conductivity of the phosphosilicate/PA phase is very stable during testing for 120 h at 250 °C (Fig.13B). Matsuda et al studied the conductivity of phosphosilicate gels with different P/Si ratio and reported a stable proton conductivity of 1×10^{-2} S cm^{-1} at 150 °C and 0.4% RH for the gel with a P/Si mole ratio of 1.0 to 1.5[27]. XRD and MAS-NMR studies showed that phosphosilicate gels can hold large amount of phosphorus and the Si-O-P-OH groups in the phosphosilicate gels enhance the retention of the adsorbed water, thus resulting in high conductivity at high temperature and low RH[27]. The much higher proton conductivity of the *in situ* formed phosphosilicate phase, as compared to the pure phosphosilicate phase, is an indicative of the retention of a large amount of PA in the *in situ* formed phosphosilicate phase, similar to the phosphosilicate gels[27, 28]. On the other hand, the excellent stability of the *in situ* formed phosphosilicate phase, as compared to the mixed PA and phosphosilicate phase (i.e., phosphosilicate+PA), implies the presence of PA/phosphosilicate nanoclusters (NCs), formed during the *in situ* formation of the phosphosilicate phase. The PA/phosphosilicate NCs are capable of holding significant amount of PA, which is responsible for the excellent proton conductivity and stability, as demonstrated in this study.

TEM and SAXS analysis showed the disintegration of the mesoporous structure of the impregnated PWA-*meso*-silicate along with the detection of phosphosilicate phase within the PBI matrix (Fig.8), indicating the *in operanto* or *in situ* formation of phosphosilicate between *meso*-silica and PA within the PBI matrix during the stability testing at 200 °C. The exceptional performance, stability in proton conductivity, and low ohmic resistance of the PA/PBI/PWA-*meso*-silica membrane fuel cell measured at 200 °C at a constant current load of 200 mA cm^{-2} (Figs.7-9) implied that the formation of an *in situ* phosphosilicate phase within the PBI membrane is also capable of holding a large amount of PA, forming PA/phosphosilicate NCs, similar to those discussed above. As PA/phosphosilicate NCs are formed *in operanto* in the PBI polymer matrix during the fuel cell operation, the connectivity at the interface between the nanocluster and PBI polymer matrix phase would be excellent. This appears to be supported by the smooth surface and no cracking of the composite membranes after testing at 200 °C for 2700 h (Fig.10A). The PA/phosphosilicate NCs can hold a significant amount of PA molecules, thereby stabilizing PA and preventing acid leaching. This explains the high stability of the proton conductivity of PA/PBI/PWA-*meso*-silica composite membranes as compared to pristine PA/PBI membranes. On the other hand, PWA may play a role in the proton conductivity of the composite membranes and compensate the conductivity loss of the composite membrane due to the low PA uptake[29]. A failure to detect the tungsten in the composite may be due to the trace amount of PWA after the disintegration of the mesoporous silica structure. In conclusion, the results indicate that the fundamental reason for the high thermal stability, high proton conductivity and excellent stability of PA/PBI/PWA-*meso*-silica composite membrane fuel cells at 200 °C is the *in situ* formation of PA/phosphosilicate NCs, as illustrated schematically in Fig.14.

The dominant factor for the fast degradation of pristine PA/PBI membrane cells is the accelerated leaching rate of PA at high temperatures[7, 30]. In addition to agglomeration of the Pt catalyst associated with the dissolution and re-deposition of Pt particles induced by high temperatures and current loadings[31, 32] and carbon corrosion[33], acid in the electrode catalyst layer also induce grain growth and agglomeration of Pt catalysts in the case of the PA/PBI based membrane cell. This is supported by the observed significant agglomeration of Pt nanoparticles particularly in the cathode layer (Fig.11 and Table 2), which is partially responsible for the performance degradation of the PA/PBI membrane fuel cell at high temperature[34]. Liu et al. revealed that extra PA in the electrodes resulted in the drastic degradation in performance and reduced stability of PA/PBI membrane fuel cells [35]. The formation of PA/phosphosilicate NCs stabilizes the acid at high temperature, diminishing the detrimental influence of acid on the agglomeration of Pt nanoparticles of PA/PBI/PWA-*meso*-silica composite membrane fuel cells. This is exactly the case as indicated by the significantly reduced grain growth of Pt particles in the case of the PA/PBI/PWA-*meso*-silica composite membrane cell (see Fig.11).

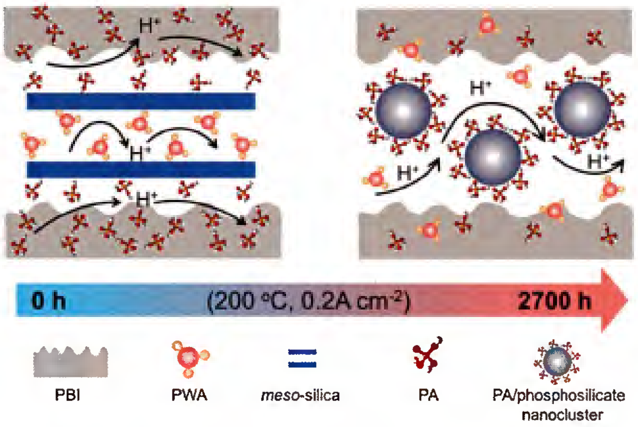

Figure 14. Scheme for the formation of PA/phophosilicate cluster structures and its role in the stabilization of PA and the proton conduction of PA/PBI/PWA-*meso*-silica composite membranes at elevated high temperature of 200 °C.

3.2. FORMATION OF PHOSPHOSILICATE PHASE IN THE COMPOSITE MEMBRANES

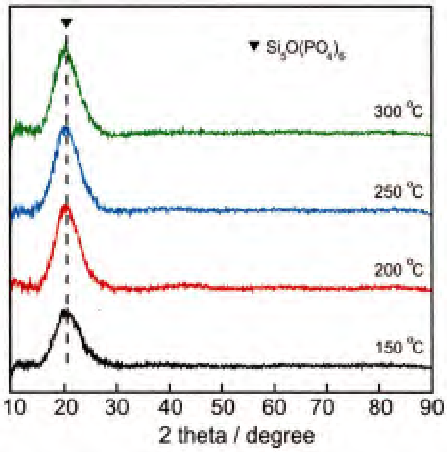

Figure 15. XRD profiles of PA/PBI composite membranes with 15 wt% PWA-*meso*-silica fillers after heat treatment at different temperatures for 24h.

The formation process of phosphosilicate phase in the PA/PBI/PWA-*meso*-silica composite membrane was studied as a function of heat-treatment temperatures for 24 h. Figure 15 shows the XRD profiles of composite membranes after heat-treated at different temperatures. For the membranes treated at temperature range of 150-300 °C, a new peak around 20 °C, which is associated with phosphosilicate phase, $Si_5O(PO_4)_6$ (SiP), was identified and its intensity increases with the heat-treatment temperature. This indicates the transformation of PA to phosphosilicate via the reaction between the doped PA and silica in the composite membranes occurs under the HT-PEM fuel cell operation conditions.

The formation temperature for the SiP phase was also investigated in the mixture of PA and mesoporous silica powder. Figure 16 is the XRD of the mixture powder sintered at different temperatures. A broad XRD peak was observed for the mixed powder sintered at 150 °C and 200 °C, while sharp and characteristic peaks associated with $Si_5O(PO_4)_6$ appear at temperatures higher than 200 °C. This indicates that crystalline phosphosilicate phase tends to be formed at temperatures higher than 200 °C. Compared with the XRD curved of SiP phase in the PA/PBI/PWA-*meso*-silica composite membrane (Fig. 15), the XRD peak intensity of the SiP phase in the PA/*meso*-silica mixed powder is much higher and clearly separated. This may indicate that crystallization of phosphosilicate phase is retarded in the PBI polymeric matrix. However, the increase of the peak intensity around 20 °C of PA/PBI/PWA-*meso*-silica composite membrane and clear identification of phosphosilicate phase of the PA/*meso*-silica mixed powder indicate the *in situ* formation of phosposilicate phase in the PA/PBI/PWA-*meso*-silica membrane but existed as nanoclusters, as discussed above.

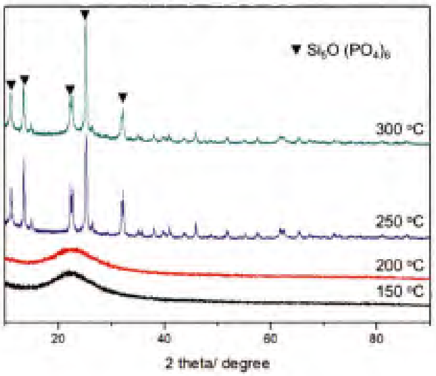

Figure 16. XRD patterns of the PA/*meso*-silica mixture sintered at different temperatures.

Figure 17 shows the SEM micrographs of phosphosilicate powder before and after acetone treatment. Phosphosilicate powder was synthesized by heat-treatment of mixture of PA and mesoporous silica (SBA-15) at 250 °C for 24 h. EDS analysis confirms that acetone washing removes phosphoric acid (PA) component from the as-synthesized PA/SiP, supported by the substantial drop of the P element intensity after acetone treatment (Fig.18). The surface of as-synthesized PA/SiP powder before acetone washing is characterized by flower-like plates (Fig.17A). However, after the PA/SiP composite material was washed by acetone, excess PA was removed (Fig.18B). SiP phase consists of rod-like particles and thin plates disappear (Fig. 17B). The particles are in the range of 0.5-1 μm and are smooth without typical mesoporous structure of original *meso*-silica precursor (Fig.17C). XRD patterns shows the presence of the identical characteristic $Si_5O(PO_4)_6$ peaks between 20 – 30 ° in both SiP powders before and after acetone washing (Fig.17D), indicating that the flow-like plates may consist of phosphoric acid crystal and SiP phase in the form of thin layered structure. This appears to be supported by the decrease of the peak intensity after acetone washing of the powder.

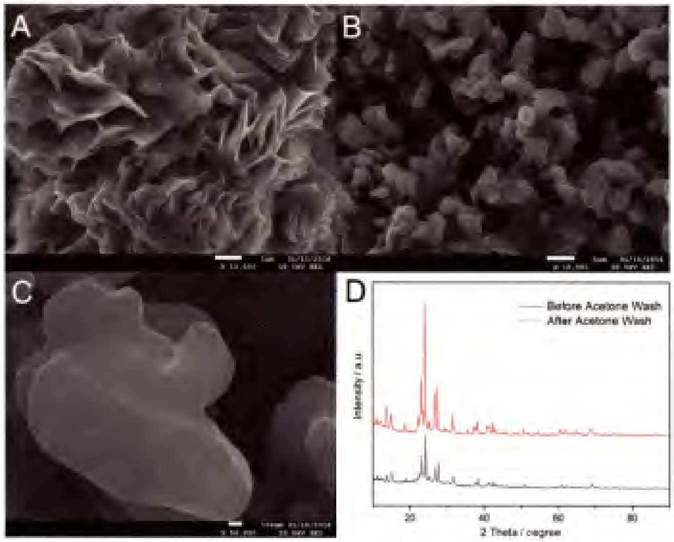

Figure 17. SEM images of the PA/phosphosilicate composites synthesized at 250 °C before (A) and after (B,C) acetone washing. Corresponding XRD curves of the composite powder were given in (D).

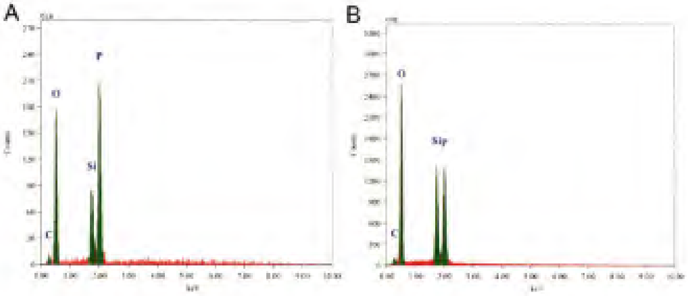

Figure 18. EDS curves of PA/SiP before (A) and (B) after acetone washing.

The proton conductivity of the SiP phase was measured by electrochemical impedance spectroscopy technique and the results are shown in Fig.19. SiP powder with or without PA was pressed into disk and sandwiched by two carbon electrodes. The proton conductivity of the PA/SiP is 0.15 S cm^{-1} at 100 °C, and increases to 0.38 S cm^{-1} at 300 °C. However, when PA was removed by acetone washing, the proton conductivity of the pristine SiP substantially drops to 1-3.6 × 10^{-3} S cm^{-1} and does not change significantly with the temperature. The results show that the high proton conductivity of the PA/SiP is due to the attached PA on the surface of the SiP particles. This again confirms the *in situ* formation of PA/phosphosilicate nanoclusters within the PA/PBI/PWA-*meso*-silica composite membrane, as schematically shown in Fig.14.

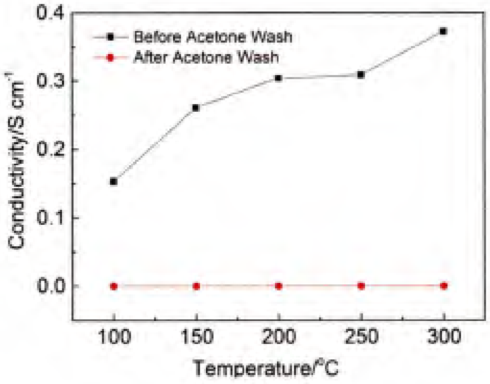

Figure 19. Proton conductivity of the SiP phase before and after acetone treatment.

3.3. EFFECT OF HEAT-TREATMENT ON PERFORMANCE OF PA/PBI/SiO_2 COMPOSITE MEMBRANE CELLS

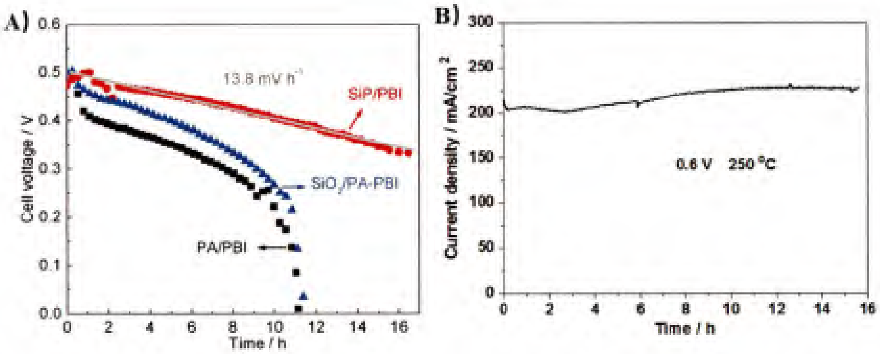

Figure 20. Performance stability of (A) pristine PA/PBI membrane and SiP/PBI composite PA/PBI composite membrane cells at 400 mA cm^{-2} and (B) SiP/PBI composite PA/PBI composite membrane cells at 0.6 V under anhydrous condition. SiO_2/PA-PBI composite without heat treatment was employed as a control group. Test conditions: Pt catalyst loading: 0.94 mg cm^{-2}; H_2 and O_2: 50SCCM; Temperature: 250°C; RH: 0%.

Figure 20 shows performance stability of a conventional PA/PBI membrane cell and SiP/PBI (with 15 wt.% *meso*-silica) membrane cells measured at 250 °C under a constant discharge current of 400 mA cm^{-2} or under a constant cell voltage of 0.6 V. SiP/PBI membrane cells were treated in PA and heat-treated at 250°C for 24 h before the test. A SiO_2/PA-PBI membrane cell without pre-heat treatment was employed as a control group. As expected, the conventional PA/PBI membrane cell cannot be operated at 250 °C due to the significant leaching and rapid decomposition of PA. The cell performance of SiO_2/PA-PBI composite membrane without pre-treatment also shows the rapid degradation, similar to the pristine PA/PBI membrane cell at

250 °C. The results clearly indicate that the simple addition of SiO_2 in PA/PBI membrane will not hinder the leaching and rapid decomposition of PA. On the other hand, the cell performance of SiP/PBI at 250 °C is much more stable. Though there is a gradual decrease in cell performance, the polarization potential does not show the characteristic rapid drop in potential associated with pristine PA/PBI membrane cells. The reason for the gradual degradation in performance is not clear at this stage, however, such decrease in the performance could also be caused by the deterioration in the Pt based electrocatalysts at high discharge current. This appears to be supported by the much stable performance of the cell under a constant cell voltage of 0.6 V (Fig.20B). The cell operated at 200 mA cm^{-2} showed a high stability and its performance became a slightly better with the polarization time.The results clearly demonstrate that the prior formation of phosphosilicate phase in the PA/PBI composite membrane significantly enhances the performance stability of PA/PBI membrane cells at 250 °C, indicating that PA/PBI/SiO_2 membrane cells can be operated at 250°C, a significant advantage of PA/PBI/SiO_2 membrane cells as compared to the current PA/PBI based PEMFCs.

3.4. CONVENTIONAL SiO_2 POWDER BASED COMPOSITE MEMBRANE CELLS

3.4.1. PERFORMANCE OF PA/PBI/SiO_2 COMPOSITE MEMBRANE CELLS

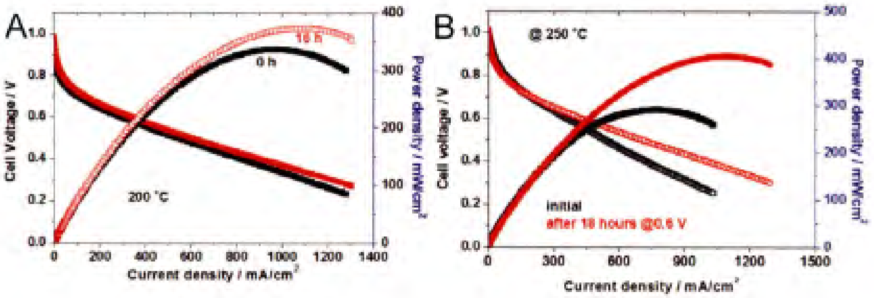

Figure 21. Polarization performance curves of the PA/PBI/SiO_2 membrane fuel cells as a function of polarization time at (A) 200 °C and (B) 250 °C. The size of silica powder was 30nm.

Mesoporous silica in the PA/PBI/meso-silica composite membranes was replaced by conventional silica powder with particle size of 30 nm. Figure 21 shows the cell performance of PA/PBI/SiO_2 composite membrane cells as a function of polarization time at 200 and 250 °C. The PA/PBI/SiO_2 composite membrane was heat-treated at 250 °C for 24 h to form phosphosilicate (SiP), phase prior to the test. The performance of the PA/PBI/SiP composite membrane cells increases initially with the polarization time, indicating the stability of the cells at 200 and 250 °C. The initial peak power density (PPD) of the PBI/SiP membrane fuel cell was 338 mW cm^{-2} at 200 °C and increased to 381 mW cm^{-2} after polarization at 200 °C for 16 h (Fig.21A). At operation temperature of 250 °C, PPD of the cell also increased from 293 mW cm^{-2} to 410 mW cm^{-2} after operating at 250 °C for 18 h (Fig.21B), which is 40 % higher than that of the initial PPD. The stable and increased performance of PA/PBI/SiO$_2$ composite membrane cells indicate the formation of PA/posphosphosilicate nanocluster between PA and SiO$_2$ particles, similar to that observed between PA and *meso*-silica. Use of silica powder will significantly reduce the cost of silica precursors. Thus, in following sections, the performance of the PA/PBI/SiO$_2$ composite membrane cells will be investigated.

3.4.2. CO RESISTANCE OF THE COMPOSITE MEMBRANE CELLS AT HIGH TEMPERATURES

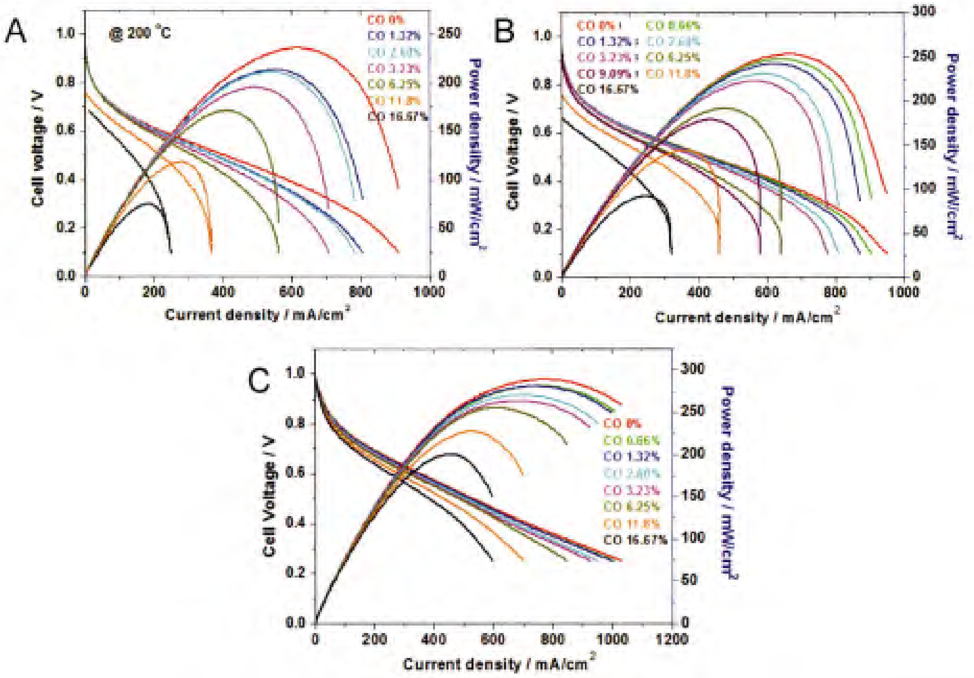

Figure 22. Polarization performance of PA/PBI/SiO$_2$ (30nm) membrane cells measured in different CO concentration in the H$_2$ fuel (A) 200 °C, (B) 230 °C and (C) 250 °C.

Increasing the operating temperature of PEMFCs will increase the CO resistance of Pt-based electrocatalysts, as shown by Li et al. on the significantly increased CO resistance of Pt at 200 °C[36]. However, the CO resistance behaviour of Pt-based elecrocatalysts at temperatures higher than 200 °C was seldom investigated. Figure 22 shows the cell performance of PA/PBI/SiO$_2$ composite membrane cells in wide range of CO-containing H$_2$ fuels at 200 - 250 °C. The PPD of the PA/PBI/SiO$_2$ membrane cell is 235.8 mW cm^{-2} at 200 °C in pure H$_2$, but decreases with the increasing in the content of CO in the H$_2$ fuel (Fig. 22A). When 16.7% CO was added, the PPD of the cell declined to 75.1 mW cm^{-2}, which is only 32 % of that of the cell operating in pure H$_2$. The is contributed to the significant adsorption of excess amount of CO on the surface of the Pt catalysts, poisoning electrocatalytic activity of Pt and thus decreasing the cell performance, in addition to the dilution of H$_2$ fuel with the addition of the high amount of CO. When the operating temperature increased to 230 °C, the PPD of the cell with pure H_2 increased to 253 mW cm^{-2}, indicating that the increase of the temperature improves the kinetics of the electrochemical reactions. However, the PPD decreases to 92 mW cm^{-2} when the CO content increases from 0 % to 16.7% (Fig.22B), which is 36 % of that in pure H_2. In the case of cells tested at 250 °C. PPD of the cell is 280 and 200 mW cm^{-2} in pure H_2 and in 16.7%CO-83.3%H_2, respectively. The power density of the cell with 16.7% CO in H_2 at 250 °C is ~71% of that in pure H_2 and is substantially higher than 32% and 36% of that measured at 200 and 230 °C, respectively. This clearly demonstrates the substantial enhancement effect of the operation temperature in the CO tolerance of PEM fuel cells. In both PPD and in powder density at 0.6 V, the decrease in the power output of the composite membrane cells is much smaller for the cell operated at 250 °C, as compared to that at 200 and 230°C (see Fig.23).

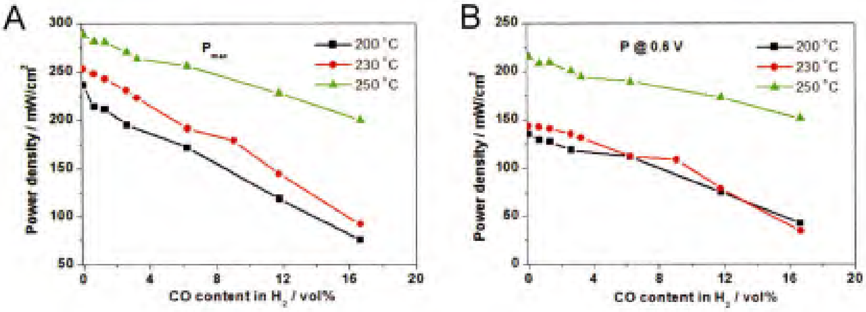

Figure 23. Power output of PA/PBI/SiO_2 (30nm) composite membrane cells measured at different temperatures as (A) PPD and (B) power density at 0.6 V.

Besides the power density performance, the increase of the operating temperature also improves the open circuit voltage (OCV) of the PA/PBI/SiO_2 composite membrane cells with in CO-containing H_2 fuel. As shown in Fig.24, the OCV of the PA/PBI/SiO_2 membrane cell remains constant at 0.9V when the CO content is lower than 3.23 %. However, the OCV drops with the increase of CO content, reduced to 0.7 V when the CO content reaches 16.7 %. The decrease of the OCV is most likely due to the oxidation of CO that is adsorbed on Pt. When the fuel cell is fed by the mixture of CO and H_2, both CO and H_2 molecules would be adsorbed at the active sites of Pt. Because the oxidation potential of CO is more positive than that of the H_2 oxidation, the excess of adsorbed CO would lead to the decrease of the OCV. When the fuel cell operating temperature increased to 230 °C, the CO content in H_2 with the stable cell OCV at 0.9 V also increased to 6.25%. However, when the operating temperature increases to 250 °C, the OCV remains at 0.9 V with the CO content in the range of 0 % to 16.7 % in H_2. The substantially increased OCV stability at high CO concentration demonstrates that the high temperature alleviates the adsorption issues of CO on Pt.

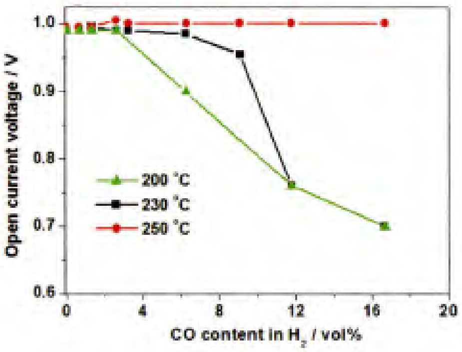

Figure 24. Plots of open circuit voltage of PA/PBI/SiO_2 composite membrane cells measured in CO containing H_2 as a function of CO concentration at different temperatures.

The performance of PA/PBI/SiO_2 composite membrane cells in CO containing H_2 appears to depend on the operating temperatures. Figure 25 shows the cell performance evaluated at temperatures from 200 °C to 260 °C in 6.25%CO in H_2. The OCV of the cell is stable at 1.0 V in the temperature range studied. The PPD of the cell is 172 mW cm^{-2} at 200 °C and increases with the operating temperature, reaching the highest value of 227 mW cm^{-2} at 240 °C. The increase of the cell performance is most likely due to the reduced adsorption and poisoning of CO on Pt electrocatalysts and increased reaction kinetics. However, with further increase in the operating temperature, the PPD decreases to 205 mW cm^{-2} at 260 °C. The stale OCV indicates that decline of the cell power output is not due to the presence of CO in H_2. Nevertheless, the exact reasons for such performance dependence on temperature are not clear at this stage.

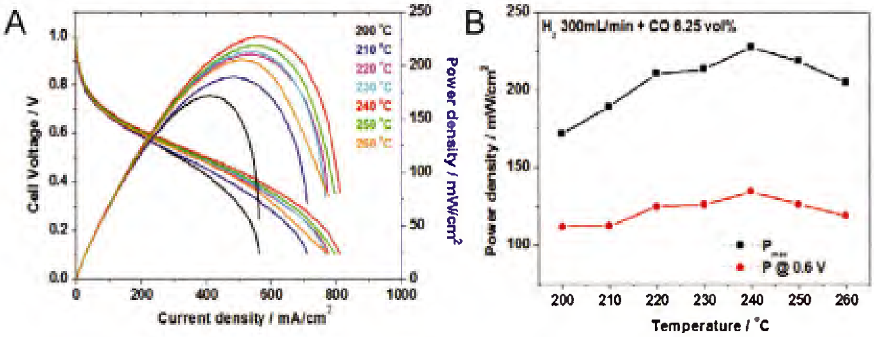

Figure 25. Performance of the PA/PBI/SiO_2 (30nm) composite membrane cells in 6.25% CO+H_2 at a flow rate of 300 SCCM (A) I-V curves and (B) peak power density and power density at 0.6 V.

Figure 26 shows the preliminary stability of PA/PBI/SiO_2 composite membrane cells in 6.25% CO/H_2 fuels under a constant cell voltage of 0.6 V, measured at 200, 230 and 240 °C. The cell current density under pure hydrogen is around 320 mA cm^{-2}, and decreased significantly to 161 mA cm^{-2} when 6.25% CO was introduced to H_2 (Fig.26A). The performance also decreases with the polarization time, reaching 127 mA cm^{-2} after 10 h operation. The cell performance is improved as the temperature increase to 230 °C. The cell was stabilized at 360 mA cm^{-2} in pure H_2 at 230 °C. Despite the initial drop of the current density to 250 mA cm^{-2} after the introduction of 6.25% CO, the cell performance showed a slightly increase to 280 mA cm^{-2} after polarization for 10 h, indicating the high stability at 230 °C. This is in contrast to the performance decrease observed on the cell at 200 °C. Similar performance stability was also observed at 240 °C. At 240 °C, the cell performance is essentially stable in the CO concentration range of 1.3% to 11.7% (Fig.26B). These results indicate the increase of the temperature could significantly increase the CO tolerance of Pt based electrocatalysts.

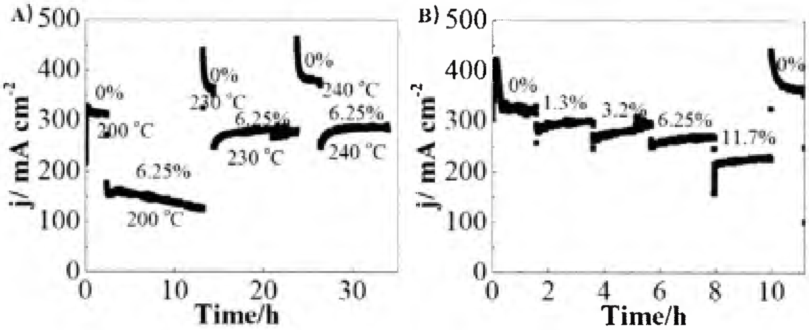

Figure 26. Stability of PA/PBI/SiO_2 composite membrane cells measured (A) in 6.25%CO/H_2 at 200, 230 and 240 °C and (B) at 230 °C in different CO concentration in H_2.

3.4.2. DIRECT METHANOL FUEL CELLS BASED ON PA/PBI/SiO_2 COMPOSITE MEMBRANES

In direct methanol fuel cells (DMFCs), one of the critical issues is the very low reaction kinetics of the Pt-based electrocatalysts for the methanol oxidation reaction (MOR) and strong adsorption and poisoning of the intermediate during MOR on the Pt catalyst, leading to the low power output of Nafion membrane based cells[37, 38]. Thus, increasing the operating temperature is expected to significantly increase the performance of the DMFCs. Figure 27 shows the performance of PA/PBI/SiO_2 composite membrane cells in liquid methanol fuel at temperatures ranging from 160 °C to 250 °C. Methanol solution of 0.25 M was directly fed to the anode at a flow rate of 0.7 mL min^{-1}. The PPD of the composite membrane cell increases with the operating temperature. PPD is 67 mW cm^{-2} at 160 °C and increases significantly to 137 mW cm^{-2} at 240 °C (Fig.27A). This is substantially higher than 20-30 mW cm^{-2} obtained on Nafion membrane based cells at room temperatures[38]. The OCV of the cell also increased from 0.67 V at 160 °C to 0.78 V at 250 °C, as shown in Fig. 27B. The increase of the PPD and OCV of the cell can be attributed to the alleviation of CO adsorption on the Pt nanoparticles and substantially increased reaction kinetics of MOR. At 250 °C, the PPD of the cell decreases slightly to 130 mW cm^{-2}, similar to the cell behaviour in CO/H_2 fuel. The result clearly demonstrates the significant advantages of the high operation temperatures in the increase of power output of DMFCs.

The durability of PA/PBI/SiO_2 composite membrane cells in methanol fuel was also evaluated under a constant cell voltage of 0.4 V at 230 °C and the results are shown in Figure 28. After operated for 4.5h, the current density of the cell slightly decreases to 131 mA cm^{-2}, which is 27.1% lower than the initial performance of the DMFC. The reason for the stability deterioration is not clear and requires further investigation.

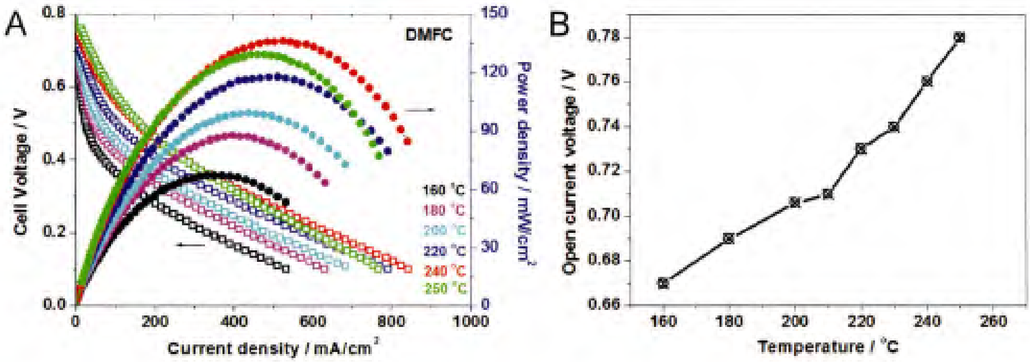

Figure 27. (A) Polarization performance and (B) open circuit voltage of PA/PBI/SiO_2 (15nm) composite membrane cells in methanol, measured at different temperatures. The flow rate of the methanol was 0.7 mL min^{-1}, and the concentration of the methanol is 25 M.

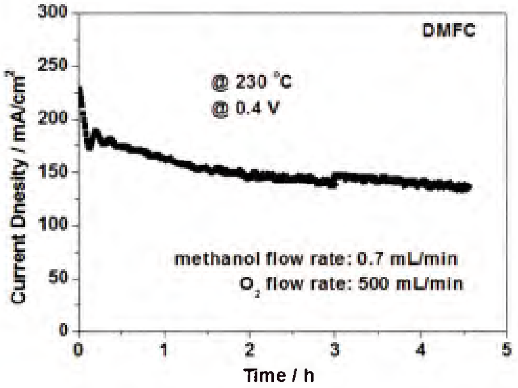

Figure 28. Durability of the PA/PBI/SiO_2 (15nm) composite membrane cells in methanol fuel under a constant cell voltage of 0.4 V at 230 °C.

3.4.3. THE EFFECT OF SiO_2 PARTICLE SIZE

SiO_2 powder with two different particle size, 15 and 30 nm, was used to study the effect of the SiO_2 particle size on the performance of PA/PBI/SiO_2 composite membrane cells. Figure 29 shows the performance of the composite membrane cells prepared with the SiO_2 particles of 15 and 30 nm. The PPD of the cells prepared with 30 nm SiO_2 is higher than that of the cell with 15 nm SiO_2. The PPD of the cell with 30 nm SiO_2 is 168 mW cm^{-2} at 240°C, which is significantly better than 137 mW cm^{-2} of the cell prepared with 15 nm SiO_2 under the same test condition. Moreover, the PPD of PA/PBI/SiO_2 (30 nm) composite membrane cells increases to 190 mW cm^{-2} at 250 °C and 204 mW cm^{-2} at 260 °C (Fig.29B), very different from the decrease of PPD of the composite cell with 15 nm SiO_2 (Fig.29A). The results indicate that the particle size of the silica additives affects the polarization performance as well as the optimum operation temperature of the cells.

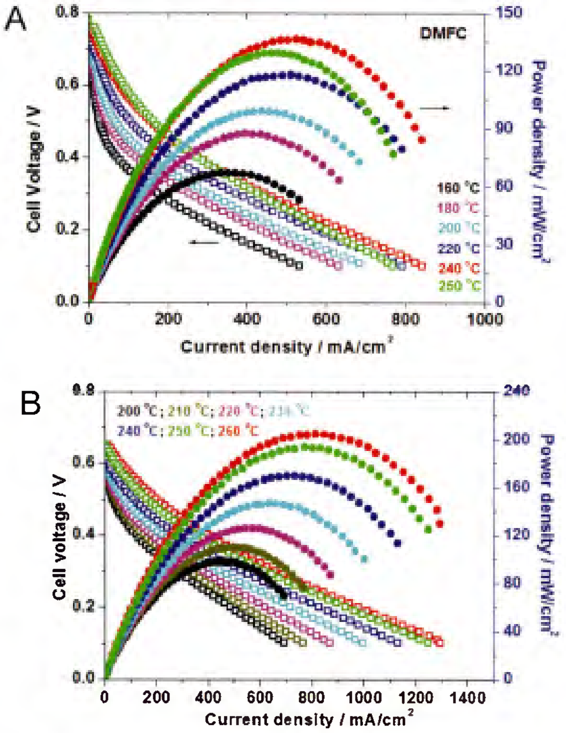

Figure 29. Polarization curves of PA/PBI/SiO_2 prepared from silica powder with (A) 15 nm and (B) 30 nm in methanol fuel at different temperatures.

Figure 30 shows the electrochemical impedance spectra of the PA/PBI/SiO_2 membrane cells in methanol fuel measured at 0.4 V. The overall cell ohmic resistance (R_Ω), measured from the intercept of high frequencies is constant at temperature range studied in both cells, while the overall cell polarization resistance (R_p) measured from the difference of the intercept of high and low frequencies changes significantly with the temperature. In the case of PA/PBI/SiO_2 (15 nm) membrane cells, R_p decreased with the temperature and reached the minimum value at 220 °C, but it increased again with the increase of temperature to 240-250 °C. This indicates that the decreased PPD of the PA/PBI/SiO_2 (15 nm) membrane cells at 250°C is due to the increase in R_p. On the other hand, R_p of the PA/PBI/SiO_2 (30 nm) membrane cells decreases with the increase of the operation temperature in the temperature range of 200 °C to 260 °C. The results indicate that the size of the silica additives may play an important role in the performance and stability of the Pt based electrocatalysts for electrode reaction in both air and fuel side. Fundamental understanding of the relationship between the silica particle size or microstructure, the formation of phosphosilicate phase and the distribution of PA/phosphosilicate nanocluster could further significantly improve the performance of he composite membrane cells in methanol fuels.

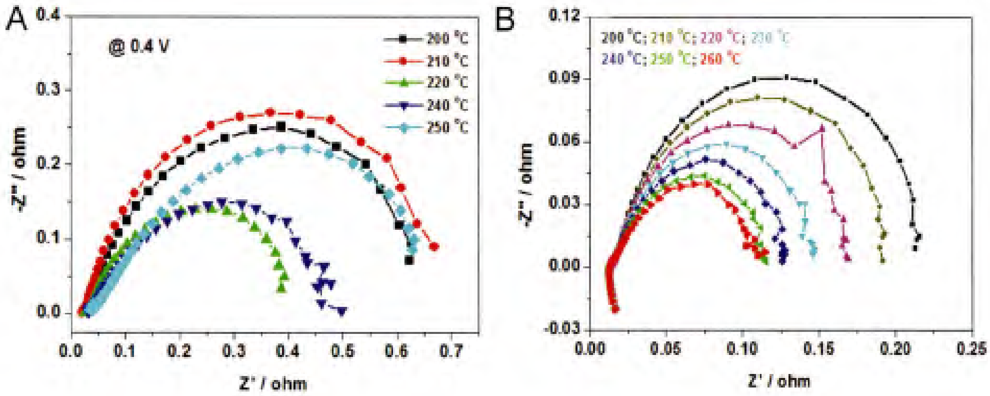

Figure 30. Electrochemical impedance spectra of the PA/PBI/SiO_2 composite membrane cells prepared with (A) SiO_2 (15 nm) and (B) SiO_2 (30 nm) at 0.4V at different temperatures.

Figure 31 shows the preliminary stability of the PA/PBI/SiO_2 (30 nm) membrane cells in methanol under a current load of 0.2 A cm^{-2} at 230 °C. The results show that the cell voltage was stable at 0.41 V, indicating the promising stability of the composite membrane cell at such high operation temperature.

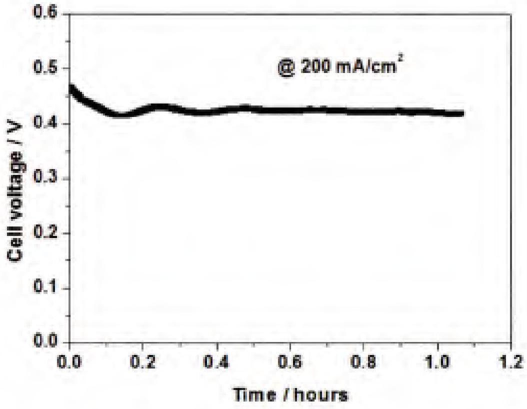

Figure 31. Preliminary stability of PA/PBI/SiO_2 (30 nm) membrane cells in methanol, measured at 230 °C under a constant current of 200 $mAcm^{-2}$. (C_m=25 mol L^{-1}, methanol flow rate of 0.5 mL min^{-1}, O_2 flow rate of 500 mL min^{-1}).

4. PART II – PRELIMINARY RESULTS OF PA/PBI/SnO_2 COMPOSITE MEMBRANE CELLS

4.1. MICROSTRUCTURE AND PROTON CONDUCTIVITY OF PA/PBI/SnO_2 COMPOSITE MEMBRANES

In addition to silica, tin oxides (SnO_2) were used as additive to the PA/PBI composite membranes, forming in situ tin pyrophosphate proton conducting carrier, similar to phosphosilicate phase in the case of PA/PBI/SiO_2 composite membranes. The fabrication of PA/PBI/SnO_2 composite membranes were more or less the same as that of PA/PBI/SiO_2 composite membranes. Figure 32 shows the optical photograph of an as-synthesized PA/PBI/SnO_2 composite membranes before and after PA loading. SnO_2 loading in the composite membrane was 10wt.%. The PBI/SnO_2 membrane is transparent, smooth and without aggregations (Fig.32A), indicating that SnO_2 is homogeneously distributed in the polymer matrix. After the PA doping, the membrane is intact and homogeneous, and there is no visible change in the morphology of the PA/PBI/SnO_2 membrane (Fig.32B). The PA uptake of the membrane was 262 wt.% and, which is 23.1% lower than that of the pristine PBI membrane.

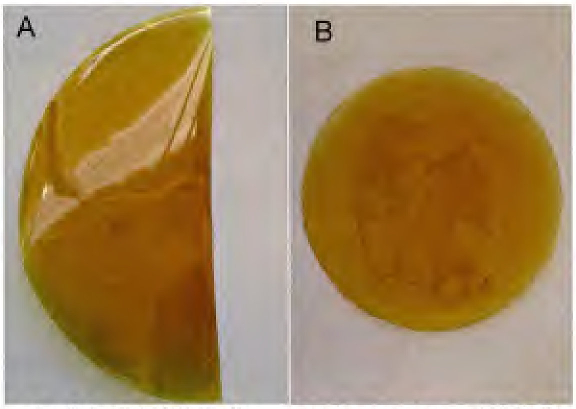

Figure 32. Optical photograph of the PA/PBI/SnO_2 composite membrane (A) before and (B) after PA doping. The loading of the SnO_2 is 10 wt.%.

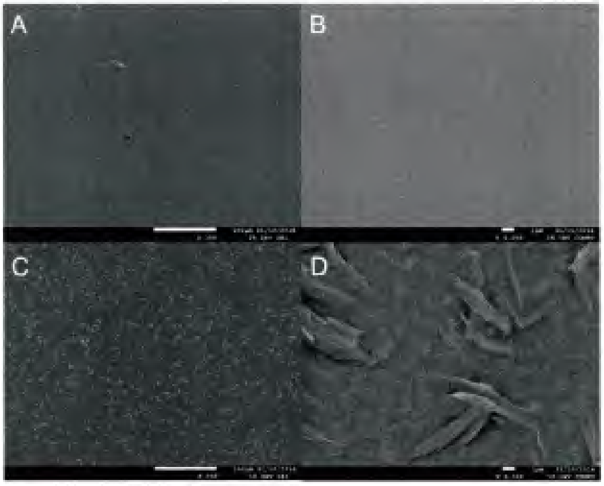

Figure 33. SEM images of the PA/PBI/SnO_2 composite membrane before (A, B) and after (C, D) heat treatment at 200 °C for 24 h.

Figure 33 shows the SEM images of the PA/PBI/SnO_2 composite membrane before and after the heat treatment. The surface of PA/PBI/SnO_2 composite membranes is smooth without aggregates (Fig.33A and B), indicating that the SnO_2 nanoparticles are well distributed in the PBI membrane. After the heat treatment of the SnO_2/PA-PBI composite membrane at 200 °C for 24 h, large amount of needle-like rods/particles were observed on the surface of the membrane (Fig.33C). Moreover, the roughness of the membrane surface is significantly increased (Fig.33D).

The phase of the PA/PBI/SnO_2 composite membrane after the heat treatment at 200°C for 24 h was characterized by XRD and the results are shown in Fig.34. After the heat treatment at 200 °C, two new peaks around 19.1° and 22.8° were observed, which can be associated with tin pyrophosphate, SnP_2O_7, in the PA/PBI/SnO_2 (SnP/PBI) membrane. This indicates the *in situ* formation of tin pyrophosphate phase between the doped PA and SnO_2 in the PA/PBI/SnO_2 composite membranes:

$$SnO_2 + 2H_3PO_4 \rightarrow SnP_2O_7 + 3H_2O \qquad (2)$$

The formed tin pyrophosphate phase, SnP_2O_7, has two phase transition temperatures at 287 °C and 557 °C and is stable up to 800 °C[39].

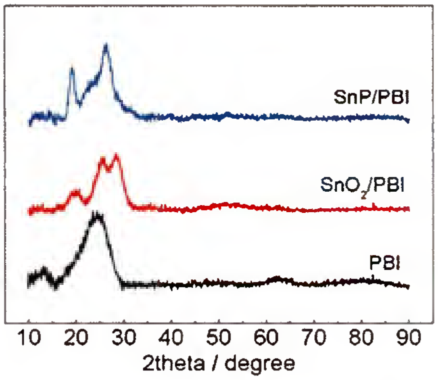

Figure 34. XRD profiles of the as synthesized PA/PBI/SnO_2 composite membrane after heat treatment at 200 °C for 24 h (denoted as SnP/PBI). Pristine PBI and SnO_2/PBI were given as control groups.

Figure 35 shows the proton conductivity of the SnP/PBI composite membrane, measured in the temperature range of 100-300 °C. The proton conductivity of the composite membrane increases from 6.0×10^{-3} S cm^{-1} at 100 °C to 5.5×10^{-2} S cm^{-1} at 300 °C. And the activation energy for proton conductivity of the membrane is 23.0 kJ mol^{-1}. Most important, the conductivity of the SnP/PBI composite membrane increases within a time period of 120 h at 250 °C (Fig.35B), indicating the good stability of the composite membranes at elevted high temperatures of 250 °C. The high conductivity and stability of the SnP/PBI composite membranes is consistent with the reported high proton conductivity and stability of tin phosphate shows at medium temperatures[29]. The result indicates that SnP/PBI membrane shows promising proton conductivity and stability for HT-PEM fuel cell applications.

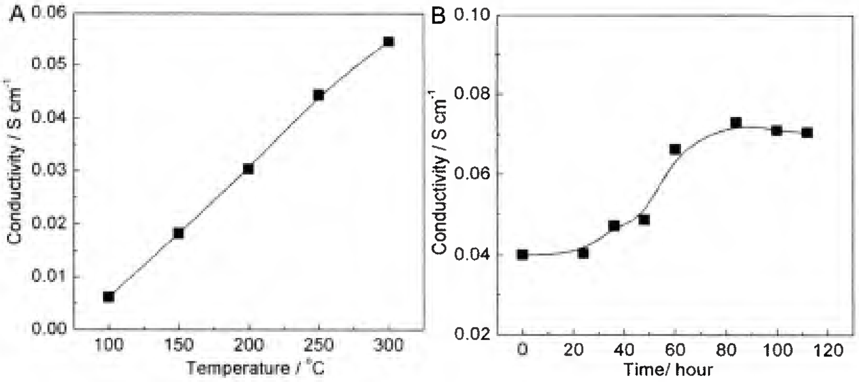

Figure 35. Proton conductivity of SnP/PBI composite membranes, measured (A) at different temperatures and (B) as a function of measurement time at 250 °C.

4.2. POLARIZATION PERFORMANCE OF PA/PBI/SNO$_2$ COMPOSITE MEMBRANE CELLS

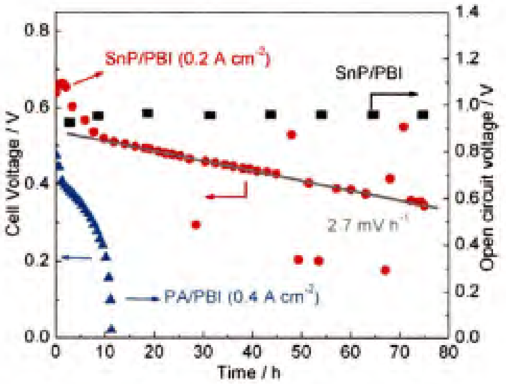

Figure 36. Performance of SnP/PBI composite membrane cells at 250 °C under a constant current of 200 mAcm^{-2} with a flow rate of H_2 50 SCCM and O_2 50 SCCM. Pt loading for both the anode and cathode was 0 9 mg cm^{-2}. Pristine PA/PBI composite membrane tested under a current of 400 mAcm^{-2} was used as the control group.

Figure 36 shows preliminary performance of a conventional PA/PBI membrane cell at 400 mAcm^{-2} and PA/PBI/SnO$_2$ (10 wt% SnO$_2$) composite membrane cell at 0.2 mAcm^{-2}, measured at 250 °C. The SnP/PBI membrane was treated at 200 °C for 24 h prior to the test. The PA loading was 330 wt% for the pristine PA/PBI membrane and 262 wt% for the SnP/PBI membrane. Conventional PA/PBI membrane cells cannot be operated at 250 °C due to the leaching and rapid decomposition of PA within 10 h. For the SnP/PBI composite membrane cell, the cell performance at 250 °C is much more stable and operated for 80 h though there is gradual decrease in the cell performance. Moreover, the OCV for the SnP/PBI membrane cell is also stable during the 80 h operation. The results clearly demonstrate the feasibility of the operation of PA/PBI/SnO_2 composite membranes cells at high temperatures of 250 °C.

DMFCs were also evaluated using SnP/PBI composite membranes and the results are shown in Fig. 37. OCV of the cell increased from 0.71 V at 200 °C to 0.74 V at 270 °C (Fig.37A). PPD of the cell increases with the increase in the temperature, achieving 170 mW cm^{-2} at 260 °C. The increase in the PPD is consistent with the reduction of R_p of the cell with the temperatures (Fig.37B).

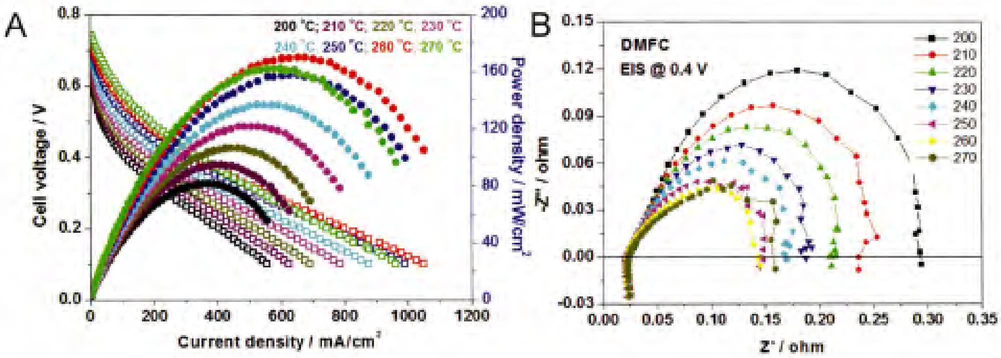

Figure 37. (A) The DMFC performance of the PBI/SnP composite membrane fuel cell under different temperatures. (B) The resistance of the cell (0.4V) at different temperatures.

Figure 38 shows the performance of the SnP/PBI composite membrane cell with different methanol flow rates at 200 °C. PPD of the fuel cell is in the range of 80 mW cm^{-2} to 83 mW cm^{-2}, measured in the methanol flow rates of 0.1-1.0 mL min^{-1}, indicating that the cell performance is independent of the flow rates. The OCV of the cell is stable at 0.7 V. The performance of PA/PBI/SnO_2 membrane cells is slightly lower than that of PA/PBI/SiO_2 composite membrane cells and this may be simply due to the fact that PA/PBI/SnO_2 membrane cells are not optimized in terms of SnO_2 content, particle size, heat-treatment temperatures, etc.

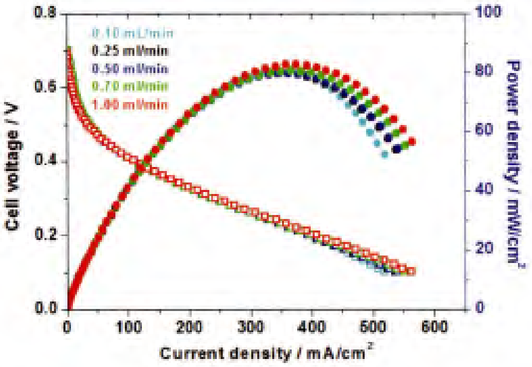

Figure 38. Polarization curves of the SnP/PBI membrane cells with different methanol flow rates at 200 °C.

Preliminary stability of the SnP/PBI composite membrane cells was evaluated at 240 °C under a current load of 0.2 A cm^{-2} and the results are shown in Fig.39. The cell was stable for 2.25 h. Though the polarization time is too short to draw the conclusion, the preliminary results are promising and warrant further work on the application of new PA/PBI/SnO_2 composite membranes in HT-PEMFCs for CO containing reformate gas and for direct methanol fuels.

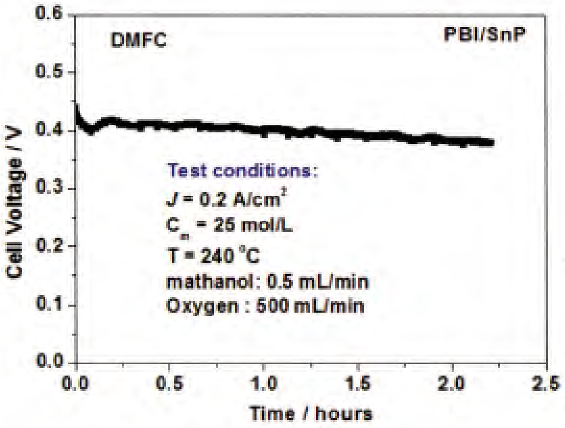

Figure 39. Preliminary stability of the direct methanol fuel cell based on the PBI/SnP composite membrane at 240 °C with a current load of 0.2 A cm^{-2}.

5. CONCLUSION

The synthesis, characterization and development of high temperature PA/PBI based PEMs with substantially improved stability at elevated high temperatures of 200-300 °C as compared to currently state-of-the-art PA/PBI PEMs have been investigated in detail in this project. The high temperature PEMs were achieved by the *in situ* formation of stabilized proton carriers or conductors such as phosphosilicate and tin pyrophosphate phases in the PBI polymeric matrix. Very different from conventional composite or hybrid inorganic/organic PEMs, the *in situ* formed phosphosilicate and tin pyrophosphate proton conductors are thermodynamically and structurally much more stable due to the intimate interface between the inorganic conductors and polymer matrix, forming metal phosphate/PA nanoclusters.

The results of the current study demonstrate that *in situ* formed metal phosphate/PA nanoclusters not only show high proton conductivity under anhydrous conditions but also stabilise the PA in polymeric matrix, thus significantly reducing the PA leaching and achieving a much better durability and higher operation temperature as compared to conventionally impregnated PA/PBI hybrid membranes. PA/PBI/SiO_2 composite membrane cells show the high tolerance to CO content in H_2 (up to 16.7%) and high performance and reasonable stability in direct liquid methanol fuel at high temperatures of 250°C. The results also show that the chemical, thermal and mechanical properties of the PA/PBI/SiO_2 composite membranes are comparable to conventional PA/PBI membranes, a significant advantage in the scale up of the fabrication process. In addition to silica, tin oxides can also be incorporated into PA/PBI, forming *in situ* tin pyrophosphate proton conducting carrier in the PBI polymer matrix. Preliminary results shows the comparable performance and stability in methanol as that of PA/PBI/SiO_2 composite membrane cells.

In conclusion, the glass transition temperature of PBI is 425 – 435 °C and the decomposition temperature for PBI in air is 580 °C. The *in situ* formed proton conductors such as phosphosilicate and tin pyrophosphate are stable up to 700 °C. Thus, in principle, the novel PEMs based on *in situ* formed metal oxide phosphate proton conductors are thermally stable at temperatures up to 200-300 °C. This has been demonstrated by the present project, showing the feasibility of new metal phosphate proton conductor modified PA/PBI based composite membranes for operation at 250°C or higher with substantial increase in the CO tolerance and power output in CO containing H_2 or in liquid methanol fuel. The preliminary results are very encourage. However, due to the time limits of the project, substantial work needs to be done to successfully develop such high temperature and liquid-fueled PEMFC as non-interrupted power sources in portable and communication electronic devices.

6. PUBLICATION

1. J Zhang, D Aili, J Bradley, HH Kuang, C Pan, R De Marco, QF Li, SP Jiang, 2017, "In situ formed phosphoric acid/phosphosilicate nanoclusters in the exceptional enhancement of durability of polybenzimidazole membrane fuel cells at elevated high temperatures", *J. Electrochem. Soc.*, **164**, F1615-F1625.
2. J Zhang, Y Cheng, J Bradley, C Pan, R De Marco, QF Li, SF Lu, SP Jiang, "Exceptional CO tolerance of new phosphoric acid polybenzimidazole/phosphosilicate composite membrane fuel cells at elevated high temperatures", in preparation.
3. Y Cheng, J Zhang, J Bradley, C Pan, R De Marco, QF Li, SF Lu, SP Jiang, "High temperature direct methanol fuel cell based on new phosphoric acid polybenzimidazole/phosphosilicate composite membranes", in preparation.

REFERENCES

[1] S.P. Jiang, X. Wang, Chapter 5. Fuel Cells: Advances and Challenges, in: V.V. Kharton (Ed.) Handbook of Solid State electrochemistry, Wiley-VCH2011, pp. 179-264.

[2] Q. Li, R.H. He, J.O. Jensen, N.J. Bjerrum, Approaches and recent development of polymer electrolyte membranes for fuel cells operating above 100 degrees C, Chemistry of Materials, 15 (2003) 4896-4915.

[3] E. Quartarone, P. Mustarelli, Polymer fuel cells based on polybenzimidazole/H3PO4, Engegy Environ. Sci., 5 (2012) 6436-6444.

[4] Q. Li, J.O. Jensen, R.F. Savinell, N.J. Bjerrum, High temperature proton exchange membranes based on polybenzimidazoles for fuel cells, Progress in Polymer Science, 34 (2009) 449-477.

[5] T. Steenberg, H.A. Hjuler, C. Terkelsen, M.T.R. Sanchez, L.N. Cleemann, F.C. Krebs, Roll-to-roll coated PBI membranes for high temperature PEM fuel cells, Energy & Environmental Science, 5 (2012) 6076-6080.

[6] J.K. Kallitsis, M. Geormezi, S.G. Neophytides, Polymer electrolyte membranes for high-temperature fuel cells based on aromatic polyethers bearing pyridine units, Polymer International, 58 (2009) 1226-1233.

[7] S. Yu, L. Xiao, B.C. Benicewicz, Durability studies of PBI-based high temperature PEMFCs, Fuel Cells, 8 (2008) 165-174.

[8] J. Mader, L. Xiao, T.J. Schmidt, B.C. Benicewicz, Polybenzimidazole/Acid Complexes as High-Temperature Membranes, Fuel Cells Ii2008, pp. 63-124.

[9] T.J. Schmidt, J. Baurmeister, Properties of high-temperature PEFC Celtec (R)-P 1000 MEAs in start/stop operation mode, Journal of Power Sources, 176 (2008) 428-434.

[10] Y. Oono, T. Fukuda, A. Sounai, M. Hori, Influence of operating temperature on cell performance and endurance of high temperature proton exchange membrane fuel cells, J. Power Sources, 195 (2010) 1007-1014.

[11] Y. Oono, A. Sounai, M. Hori, Long-term cell degradation mechanism in high-temperature proton exchange membrane fuel cells, Journal of Power Sources, 210 (2012) 366-373.

[12] Y. Oono, A. Sounai, M. Hori, Prolongation of lifetime of high temperature proton exchange membrane fuel cells, Journal of Power Sources, 241 (2013) 87-93.

[13] D. Aili, J. Zhang, M.T.D. Jakobsen, H.J. Zhu, T.Y. Yang, J. Liu, M. Forsyth, C. Pan, J.O. Jensen, L.N. Cleemann, S.P. Jiang, Q.F. Li, Exceptional durability enhancement of PA/PBI based polymer electrolyte membrane fuel cells for high temperature operation at 200 degrees C, Journal of Materials Chemistry A, 4 (2016) 4019-4024.

[14] J. Zeng, P.K. Shen, S.F. Lu, Y. Xiang, L. Li, R. De Marco, S.P. Jiang, Correlation between proton conductivity, thermal stability and structural symmetries in novel HPW-meso-silica nanocomposite membranes and their performance in direct methanol fuel cells, J. Membr. Sci., 397 (2012) 92-101.

[15] S.P. Jiang, Functionalized mesoporous structured inorganic materials as high temperature proton exchange membranes for fuel cells, Journal of Materials Chemistry A, 2 (2014) 7637-7655.

[16] J.O. Jensen, Q. Li, R. He, C. Pan, N.J. Bjerrum, 100-200 degrees C polymer fuel cells for use with NaAlH4, J. Alloy. Compd., 404 (2005) 653-656.

[17] R.H. He, Q.F. Li, G. Xiao, N.J. Bjerrum, Proton conductivity of phosphoric acid doped polybenzimidazole and its composites with inorganic proton conductors, J. Membr. Sci., 226 (2003) 169-184.

[18] G. Nawn, G. Pace, S. Lavina, K. Vezzu, E. Negro, F. Bertasi, S. Polizzi, V. Di Noto, Nanocomposite Membranes based on Polybenzimidazole and ZrO2 for High-Temperature Proton Exchange Membrane Fuel Cells, ChemSusChem, 8 (2015) 1381-1393.

[19] G. Nawn, G. Pace, S. Lavina, K. Vezzu, E. Negro, F. Bertasi, S. Polizzi, V. Di Noto, Interplay between Composition, Structure, and Properties of New H3PO4-Doped PBI4N-HfO2 Nanocomposite Membranes for High-Temperature Proton Exchange Membrane Fuel Cells, Macromolecules, 48 (2015) 15-27.

[20] Y.C. Jin, M. Nishida, W. Kanematsu, T. Hibino, An H3PO4-doped polybenzimidazole/Sn0.95Al0.05P2O7 composite membrane for high-temperature proton exchange membrane fuel cells, J. Power Sources, 196 (2011) 6042-6047.

[21] A. Shabanikia, M. Javanbakht, H.S. Amoli, K. Hooshyari, M. Enhessari, Effect of La2Ce2O7 on the Physicochemical Properties of Phosphoric Acid Doped Polybenzimidazole Nanocomposite Membranes for High Temperature Proton Exchange Membrane Fuel Cells Applications, J. Electrochem. Soc., 161 (2014) F1403-F1408.

[22] K. Tadanaga, Y. Michiwaki, T. Tezuka, A. Hayashi, M. Tatsumisago, Structural change and proton conductivity of phosphosilicate gel-polyimide composite membrane for a fuel cell operated at 180 degrees C, J. Membr. Sci., 324 (2008) 188-191.
[23] A. Matsuda, T. Kanzaki, K. Tadanaga, M. Tatsumisago, T. Minami, Proton conductivities of sol–gel derived phosphosilicate gels in medium temperature range with low humidity, Solid State Ionics, 154–155 (2002) 687-692.
[24] J. Hu, H. Zhang, Y. Zhai, G. Liu, J. Hu, B. Yi, Performance degradation studies on PBI/H3PO4 high temperature PEMFC and one-dimensional numerical analysis, Electrochim. Acta, 52 (2006) 394-401.
[25] S.P. Szu, L.C. Klein, M. Greenblatt, Effect of precursors on the structure of phosphosilicate gels: 29Si and 31P MAS-NMR study, J. Non-cryst. Solid, 143 (1992) 21-30.
[26] T. Matsui, S. Takeshita, Y. Iriyama, T. Abe, Z. Ogumi, Proton-Conductive Electrolyte Consisting of NH 4 PO 3 / TiP2 O 7 for Intermediate-Temperature Fuel Cells, J. Electrochem. Soc., 152 (2005) A167-A170.
[27] A. Matsuda, T. Kanzaki, K. Tadanaga, M. Tatsumisago, T. Minami, Medium temperature range characterization as a proton conductor for phosphosilicate dry gels containing large amounts of phosphorus, Electrochim. Acta, 47 (2001) 939-944.
[28] A. Matsuda, T. Kanzaki, M. Tatsumisago, T. Minami, Comparison of structure and proton conductivity of phosphosilicate gels derived from several kinds of phosphorus-containing compounds, Solid State Ionics, 145 (2001) 161-166.
[29] X. Xu, S. Tao, P. Wormald, J.T.S. Irvine, Intermediate temperature stable proton conductors based upon SnP2O7, including additional H3PO4, J. Mater. Chem., 20 (2010) 7827-7833.
[30] S.H. Eberhardt, T. Lochner, F.N. Büchi, T.J. Schmidt, Correlating Electrolyte Inventory and Lifetime of HT-PEFC by Accelerated Stress Testing, J. Electrochem. Soc., 162 (2015) F1367-F1372.
[31] G. Liu, H. Zhang, J. Hu, Y. Zhai, D. Xu, Z.-g. Shao, Studies of performance degradation of a high temperature PEMFC based on H3PO4-doped PBI, J. Power Sources, 162 (2006) 547-552.
[32] J.A. Bett, K. Kinoshita, P. Stonehart, Crystallite growth of platinum dispersed on graphitized carbon black, J. Catal., 35 (1974) 307-316.
[33] L.N. Cleemann, F. Buazar, Q. Li, J.O. Jensen, C. Pan, T. Steenberg, S. Dai, N.J. Bjerrum, Catalyst Degradation in High Temperature Proton Exchange Membrane Fuel Cells Based on Acid Doped Polybenzimidazole Membranes, Fuel Cells, 13 (2013) 822-831.
[34] J. Hu, H. Zhang, Y. Zhai, G. Liu, B. Yi, 500h continuous aging life test on PBI/H3PO4 high-temperature PEMFC, Int. J. Hydrogen Energy, 31 (2006) 1855-1862.
[35] S. Matar, A. Higier, H. Liu, The effects of excess phosphoric acid in a Polybenzimidazole-based high temperature proton exchange membrane fuel cell, J. Power Sources, 195 (2010) 181-184.
[36] X. Gang, L. Qingfeng, H.A. Hjuler, N.J. Bjerrum, Hydrogen Oxidation on Gas Diffusion Electrodes for Phosphoric Acid Fuel Cells in the Presence of Carbon Monoxide and Oxygen, Journal of The Electrochemical Society, 142 (1995) 2890-2893.
[37] D.Y. Chung, K.-J. Lee, Y.-E. Sung, Methanol Electro-Oxidation on the Pt Surface: Revisiting the Cyclic Voltammetry Interpretation, The Journal of Physical Chemistry C, 120 (2016) 9028-9035.
[38] S.P. Jiang, Z.C. Liu, Z.Q. Tian, Layer-by-layer self-assembly of composite polyelectrolyte-nafion membranes for direct methanol fuel cells, Adv. Mater., 18 (2006) 1068-+.
[39] R.K.B. Gover, N.D. Withers, S. Allen, R.L. Withers, J.S.O. Evans, Structure and Phase Transitions of SnP2O7, Journal of Solid State Chemistry, 166 (2002) 42-48.